AGU PUBLICATIONS

JGR

Journal of Geophysical Research: Oceans

RESEARCH ARTICLE

10.1002/2017JC012703

Key Points:

- Nonlinear energy transfers explain the group modulation influence on high and low frequency wave dynamics
- The growth of the high frequency wave skewness increases when the group frequency decreases promoting wave breaking at larger water depths
- Long wave dissipation close to the shoreline is low for long wave groups but high for the shortest wave groups suggesting long wave breaking

Correspondence to:
E. M. Padilla,
e.padilla14@imperial.ac.uk

Citation:
Padilla, E. M. and M. Alsina (2017), Transfer and dissipation of energy during wave group propagation on a gentle beach slope, *J. Geophys. Res. Oceans*, *122*, doi:10.1002/2017JC012703.

Received 14 JAN 2017
Accepted 24 JUL 2017
Accepted article online 15 AUG 2017

Transfer and dissipation of energy during wave group propagation on a gentle beach slope

Enrique M. Padilla[1] and José M. Alsina[1]

[1]Department of Civil and Environmental Engineering, Imperial College of Medicine, Science and Technology, London, UK

Abstract The propagation of bichromatic wave groups over a constant 1:100 beach slope and the influence of the group modulation is presented. The modulation is controlled by varying the group frequency, f_g, which is shown to remarkably affect the energy transfer to high and low frequency components. The growth of the high frequency (hf) wave skewness increases when f_g decreases. This is explained by nonlinear coupling between the primary frequencies, which results in a larger growth of hf components as f_g decreases, causing the hf waves to break earlier. Due to high spatial resolution, wave tracking has provided an accurate measurement of the varying breakpoint. These breaking locations are very well described ($R^2 > 0.91$) by the wave-height to effective-depth ratio (γ). However, for any given Iribarren number, this γ is shown to increase with f_g. Therefore, a modified Iribarren number is proposed to include the grouping structure, leading to a considerable improvement in reproducing the measured γ-values. Within the surf zone, the behavior of the Incident Long Wave also depends on the group modulation. For low f_g conditions, the lf wave decays only slightly by transferring energy back to the hf wave components. However, for high f_g wave conditions, strong dissipation of low frequency (lf) components occurs close to the shoreline associated with lf wave breaking. This mechanism is explained by the growth of the lf wave height, induced partly by the self-self interaction of f_g, and partly by the nonlinear coupling between the primary frequencies and f_g.

1. Introduction

The groupiness of high frequency (hf) waves, short gravity waves of period O(10 s), and the presence of associated low frequency (lf) motions, O(100 s), are characteristic features of random wave conditions propagating to the coastline. These wave features can have important implications in terms of sediment transport and beach morphology [*Aagaard and Greenwood*, 2008; *Baldock et al.*, 2011; *Alsina et al.*, 2016; *de Bakker et al.*, 2016b] or in the operability and safety of coastal infrastructures such as harbors [*Bowers*, 1977].

The presence of wave groups of short gravity waves implies the existence of at least two frequency components in the wave energy frequency distribution. These are exactly two components of similar frequency in case of bichromatic wave groups. The nonlinear interaction between different wave components causes energy transfers in the wave spectrum [*Phillips*, 1960; *Hasselmann et al.*, 1963]. Nonlinear coupling and energy transfer between components occur to frequency components above and below the primary interacting frequencies. *Biésel* [1952] presented a second-order solution for a wave system in uniform water depth consisting of the sum of a given number of elementary harmonic waves, bound superharmonics and subharmonics of pairs of interacting primary components. Later, *Phillips* [1960] and *Hasselmann et al.* [1963] presented general formulations for the generation of second-order and third-order waves resulting from the sum and difference of interacting components.

Two main generation mechanisms of lf motions by hf wave groups have been identified. One is due to the difference interactions between primary waves resulting in group-bound long waves in antiphase with the envelope of the wave groups [*Biésel*, 1952; *Longuet-Higgins and Stewart*, 1962, 1964]. Physically, this wave may be considered as the equilibrium system response to variations in the radiation stresses on the time and length scales of the short-wave groups [*Longuet-Higgins and Stewart*, 1962, 1964]. A second mechanism considers the generation of both shoreward and seaward propagating free waves during wave breaking by the spatial modulation of the breakpoint due to the wave-group structure [*Symonds et al.*, 1982; *Symonds and Bowen*, 1984]. The breakpoint mechanism has been demonstrated experimentally [*Kostense*, 1984;

Baldock et al., 2000; *Baldock and Huntley*, 2002; *Contardo and Symonds*, 2013; *Moura and Baldock*, 2017] and numerical formulations have been presented [*Schäffer and Jonsson*, 1990; *Schäffer*, 1993] for the combination of the breakpoint and the radiation stress generation mechanisms.

During wave-group propagation onto a beach, the hf wave groups and lf motions undergo substantial nonlinear transformations. The Incident Long Wave (ILW), which travels bound to the wave groups, will grow during wave-group shoaling. The mechanism proposed by [*Longuet-Higgins and Stewart*, 1964] considers a steady-state equilibrium solution, which, in principle, is no longer applicable to shoaling waves. In the equilibrium situation, which is consistent with a constant lag of π radians [*Battjes et al.*, 2004], there should not be any transfer of energy from the primary waves to the bound wave. However, during the shoaling process, the ILW has been observed to increasingly lag behind the group by an additional phase shift $\Delta\psi$ [*List*, 1992; *Van Dongeren and Svendsen*, 1997; *Janssen et al.*, 2003; *Battjes et al.*, 2004]. This progressive phase lag has been shown to be fundamental in the process of energy transfer from the primary waves. *Battjes et al.* [2004] showed that this phase lag appears to increase with increasing frequency for a given beach slope. This trend was also observed for the ILW amplitude and generalized as a function of the normalized bed slope parameter β,

$$\beta=\frac{S}{\omega}\sqrt{\frac{g}{h}}, \tag{1}$$

where S is the bed slope, ω is the angular frequency, and g is the gravitational acceleration. The water depth h is usually taken at the breaking location (h_b), which results in β_b for this case. *Battjes et al.* [2004] computed the energy transfer per frequency band, highlighting that for low values of β (they suggest $\beta_b < 0.1$), a "mild-slope regime" exists in which the forced wave amplitude growth in the shoaling zone is large and close to the shallow-water equilibrium solution $\sim h^{-5/2}$. For large values of β ($\beta_b > 0.45$) a "steep-slope regime" is defined where the amplitude growth is weak and close to a free-wave variation $\sim h^{-1/4}$ (Green's law). The parameter β has been also proposed to be inversely proportional to the ratio of the radiation stress to breakpoint long wave forcing [*Van Dongeren et al.*, 2002]. Similarly, *Baldock et al.* [2000] and *Baldock and Huntley* [2002] proposed that the breakpoint-forcing mechanism will become ineffective when the breakpoint excursion becomes large in comparison with the wavelength of the long-wave motion. According to *Baldock et al.* [2000], this occurs when $G/2\pi\beta_H > \alpha$, where G is the groupiness factor [*List*, 1991], β_H is defined by replacing h by the lf wave height H in equation (1) and α is some fraction of the wavelength of the free long wave, estimated to lie in the range 0.2–0.3.

During shoreward propagation of the primary wave components (f_1 and f_2), nonlinear coupling occurs, and causes an energy transfer to wave components with the sum (f_1+f_2) or difference (f_1-f_2) frequency. Nonlinear energy transfer to the difference frequencies is associated to the growth of the ILW during shoaling [*Janssen et al.*, 2003; *de Bakker et al.*, 2015] while energy transfer to sum frequencies results in changes in the shape of individual shoaling waves from a quasi-symmetrical profile in deep water to more skewed waves in shallow water characterized by sharp crests and flat broad troughs [*Guza and Thornton*, 1982; *Elgar and Guza*, 1985]. Along with the amplitude evolution, the phase of the different hf harmonics changes during shoaling leading to a steepening of the wave shape face. The lack of horizontal symmetry in the wave shape (i.e., sharper crests and flatter troughs) is known as skewness, whereas the lack of vertical wave symmetry or its tendency to become pitched forward is called wave asymmetry. These changes in the skewness and asymmetry of hf water surface elevations cannot be explained by linear theory. Higher-order regular wave theories, such as that by *Stokes* [1847], can predict the skewness of individual hf waves from the increasing contributions of superharmonics of the primary frequency. However, higher-order wave theories do not lead to wave asymmetry because the harmonic components of the individual hf waves remain phase-locked and in phase with the primary frequency. The pitching forward of the individual waves, or relative steepening of the wave face, is due to a forward phase-shifting of the harmonics relative to the primary components [*Elgar and Guza*, 1986; *Doering and Bowen*, 1986, 1995]. Wave skewness and asymmetry increase during shoaling and eventually the hf waves will become unstable and break.

Due to hf wave breaking, the wave energy close to the shoreline may be dominated by lf wave motions, especially on dissipative beaches. Close to the wave breaking location, when the hf waves are in shallow water, bound lf waves can also be progressively "released" from the hf wave groups since these nondispersive conditions correspond to those where the forced long wave satisfies the free wave dispersion relationship [*Elgar et al*., 1992; *Herbers et al*., 1995; *Baldock and Huntley*, 2002; *Baldock*, 2012]. Conversely, if the hf waves are not shallow water waves at the breakpoint, the ILW may reduce in amplitude along with the reduction in the primary wave forcing after breaking [*Baldock and Huntley*, 2002; *Battjes et al*., 2004; *Dong et al*., 2009; *Lara et al*., 2011; *Baldock*, 2012]. A number of experimental and field data sets suggest that ILWs undergo strong nearshore dissipation after wave group breaking [*Baldock et al*., 2000; *Battjes et al*., 2004; *Henderson et al*., 2006; *Baldock*, 2012]. Part of the nearshore lf wave dissipation has been suggested to occur through nonlinear interactions that transfer energy from the lf waves back to hf components and is not generally attributed to frictional losses [*Henderson et al*., 2006; *Thomson et al*., 2006; *Van Dongeren et al*., 2007; *de Bakker et al*., 2014]. Recently, a numerical investigation [*de Bakker et al*., 2016a] has shown that this situation is characteristic of steep sloping beach conditions where lf waves interact with the hf components transferring energy to hf components.

For some lf components and beach slope combinations resulting in small values of β, the nearshore dissipation of lf waves is attributed to long wave breaking [*Battjes et al*., 2004; *Van Dongeren et al*., 2007; *de Bakker et al*., 2014, 2016a, 2016b] suggesting lf energy saturation at the shoreline. Laboratory data [*Van Dongeren et al*., 2007] and numerical simulations [*de Bakker et al*., 2016a] have confirmed that with decreasing depth on low-sloping beach conditions the lf wave self-self interactions may dominate energy transfer causing the lf wave front to steepen and eventually break. This seems consistent with field measurements of run-up elevation [*Ruessink et al*., 1998; *Sénéchal et al*., 2011; *Guedes et al*., 2013] showing run-up energy saturation for low frequencies during highly dissipative energetic storms.

The main aim of this work is to study the wave-group propagation on a dissipative 1:100 sloping laboratory beach, with a focus on the energy transfer from primary waves to superharmonics and subharmonics due to nonlinear frequency coupling (triad interactions). The nonlinear energy transfer to superharmonics has important implications in the wave breaking process and clear evidence of a relationship between the wave breaking onset and the group frequency will be presented. As the use of a gentle beach slope causes energy dissipation of most of the hf wave components due to wave breaking and a dominance of the lf energy in the inner surf zone, the lf wave behavior during hf wave shoaling and after hf wave breaking will be also discussed.

2. Experimental Setup and Method of Analysis

2.1. Experimental Setup

The experiments presented in this study have been carried out in the Wave Evolution Flume at Imperial College London. This wave flume has a length of 60 m, with a distance from the paddles to the emerged end of 52 m. The flume width is 0.3 m with a working water depth of 0.5 m (see Figure 1). A beach profile has been built made of glass with a gentle slope (1:100).

The waves are generated using a flap-type, bottom-hinged, wave paddle which is numerically controlled with active-force feedback. This guarantees the generation of the desired waves and the absorption of any unwanted reflected waves. Wave generation is performed using a force control technique that has been shown to be effective at suppressing high frequency spurious waves [*Spinneken and Swan*, 2011]. This technique is included in the commercial software that controls the wave paddle. The software does not allow for second-order wave generation. However, for this study, we introduced an active suppression system of spurious subharmonics in the form of unwanted energy as Incident Free Long Waves (IFLWs). The suppression technique consists of a separation methodology of the incident bound and free long waves (see *Padilla*

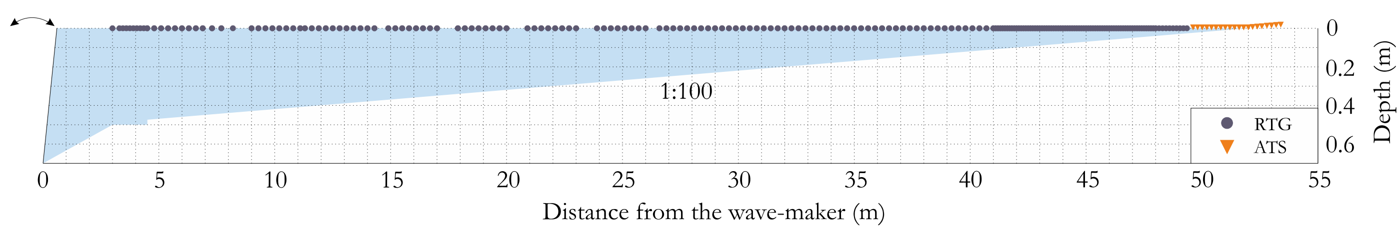

Figure 1. Cross-shore bottom profile, still water level, and instrument locations deployed from the wave paddles. Dots and triangles indicate resistive-type and acoustic-type sensors, respectively.

and Alsina [2016] for further details on the separation technique). After an initial generation, any IFLW (spurious) is separated using measured time series of water surface elevation at different cross-shore locations and, after back propagation to the wave paddle, a correction is introduced to suppress the unwanted IFLW during generation. This methodology provides in practice similar results to a theoretical second-order generation function with the inconvenience that it requires measuring and effectively correcting the wave generation each time.

The water surface elevation measuring system is composed of a set of resistance-type gauges (RTG) and acoustic-type sensors (ATS). Both type of systems have been deployed on movable platforms that, with repeated experiments, allow us to obtain a surface elevation data set with a spatial resolution from 0.3 m in the shoaling zone to 0.1 m in the surf zone. The acoustic-type sensors are used in the downstream end of the flume to characterize the water surface elevation within the swash zone. In total, this high spatial resolution allows us to obtain 218 cross-shore measuring locations along the 52 m of wave flume (see Figure 1). Additionally, the breaking process is also recorded by video images.

2.2. Dataset Description

In this work, 12 bichromatic wave cases with the same wave energy content have been studied. These are fully modulated cases ($a_1/a_2=1$) with the same initial amplitude for the primary frequencies f_1 and f_2 ($a_1=a_2=0.015$ m). The generated wave conditions are divided into three different series by modifying the mean primary frequency, $f_p=(f_1+f_2)/2$ (series *A*, $f_p=1.1$ Hz; *B*, $f_p=0.9$ Hz; and *C*, $f_p=0.6$ Hz). Consequently, the second order sum-term component is imposed and remains the same for each series. Within each series, for any chosen value of f_p (see Table 1), the wave group frequency is varied by modifying the difference frequency ($f_g=\Delta f=f_1-f_2$). Assuming that the group velocity (linear theory), c_{gp}, corresponding to the mean primary frequency, f_p, is a good approximation of the actual celerity of the wave groups [*Janssen et al*., 2003], then each wave series is characterized by a constant wave energy and energy flux but a varying wave group period.

The selection of these wave conditions, that is, the definition of the couple $[f_1, f_2]$ is made in such a way that all the groups are identical within a time series. It may be reduced to the condition $Rp=T_r/T_g=1$, where the repetition time or periodicity of the signal T_r matches the group period $T_g=1/f_g$. Thus, the relationship between $[f_p, f_g]$ and n, the number of short waves forming a group, for $Rp = 1$, is

$$f_g=\frac{f_p}{n+1/2}. \tag{2}$$

The minimum number of generated waves per group is 3, which yields the higher group frequencies from 0.314 Hz for series *A* to 0.171 Hz for series *C*. Conversely, the group frequency decreases with an increasing number of short waves in each group. For the longest generated group (length around 30 m), f_g decreases until 0.048 Hz, representing 12 individual waves per group (case *C-3*). The longest generated wave group is limited by the generation system, not being able to guarantee a proper wave absorption and a second-order correction below 0.04 Hz. Using bichromatic experimental conditions, the separation between high

Table 1. Simulated Bichromatic Wave Conditions, With f_1 and f_2 as the Primary Components, Whose Mean Frequency is f_p[a]

Case	f_p (Hz)	f_1 (Hz)	f_2 (Hz)	$\Delta f=f_g$ (Hz)	n	x_{ShWL} (m)	Δx_b (m)
A-1	1.1	1.257	0.943	0.314	3	1.9	0.6
A-2	1.1	1.200	1.000	0.200	5	1.9	1.3
A-3	1.1	1.144	1.056	0.088	12	1.9	3.2
A-4	1.1	1.127	1.073	0.054	20	1.9	4.2
A-5	1.1	1.122	1.078	0.043	25	1.9	4.7
B-1	0.9	1.029	0.771	0.257	3	2.9	0.7
B-2	0.9	0.981	0.818	0.164	5	2.9	0.8
B-3	0.9	0.936	0.864	0.072	12	2.9	3.8
B-4	0.9	0.922	0.878	0.044	20	2.9	4.4
C-1	0.6	0.686	0.514	0.171	3	6.5	0.9
C-2	0.6	0.640	0.560	0.080	7	6.5	4.5
C-3	0.6	0.624	0.576	0.048	12	6.5	6.3

[a]The difference frequency or group frequency ($\Delta f=f_1-f_2$) is f_g and n is the number of short waves in each group, whose shallow water limit is x_{ShWL}. Δx_b is the measured breakpoint excursion.

and low frequency motions is straightforward. Every wave motion at around the primary frequencies (f_1 and f_2) and higher (frequency range in the present experiments of around 0.5–2 Hz) belongs to the high frequency domain. Conversely, the wave motions at around the group frequency and below are considered as low frequency (frequency range of 0.04–0.4 Hz).

The sampling frequency is 128 Hz for RTG, decreasing to 100 Hz for ATS. The designed experiments are characterized by 12 min long data series. However, reasonably steady conditions were expected to develop along the flume only after the initial 200 s.

2.3. Data Analysis

The repeatability of the groups plays an important role in the definition of the cases. Once the water surface signal is ensemble averaged, the computed standard deviation is not higher than 3×10^{-4} m (0.75% of the significant wave height H_s), below the RTG accuracy ($\pm5\times10^{-4}$ m). Hence, to satisfy entirely $Rp=1$ and minimize noise and undesired errors, the presented surface-elevation time series are henceforth built as a repeating sequence of ensemble-averaged stationary groups. Consequently, the length of the time series may be defined as a multiple of the grouping period T_g. The used time series comprises 50 groups for frequency-discretization purposes.

Spectral analysis of the surface elevation η is performed via a fast Fourier transform (FFT). Each FFT was performed using time series resampled to 10 Hz with 2048 data points. Likewise, bispectral analysis (explained below in section 2.3.3) is performed using a total number of 8192 data points, divided into eight segments (1820 samples per segment) whose overlapping is 50% of the segment length. As a results, final estimates of the bispectrum yield a frequency resolution of 0.0049 Hz and 16 degrees of freedom.

2.3.1. Wave Separation Technique

The separation of the ingoing/outgoing waves at a certain frequency within a time series involves obtaining both the initial amplitude A_0 and phase $\phi_0=\phi(t=0, x=0)$ for the ingoing and outgoing wave components. Hereafter, we will refer to this pair $[A_0, \phi_0]$ as $Z=A_0\cdot e^{i\phi_0}$. To achieve this, there are some techniques available [*Kostense*, 1984; *Baldock and Simmonds*, 1999; *Battjes et al.*, 2004; *Van Dongeren et al.*, 2007, among others] that focus on the distribution of the wave energy budget at a given frequency *f* among the ingoing and outgoing components based on their different propagation rates along a number of adjacent wave gauges (local array).

This main separation technique, the so-called array method, has been presented for the separation of the Incident Long Wave (ILW), bound to the grouping structure, and the reflected free wave, or Outgoing Free Long Wave (OFLW), in *Battjes et al.* [2004] and *Van Dongeren et al.* [2007]. They assumed the nonexistence of any Incident Free Long Wave (IFLW), i.e., all the ILW energy propagates bound to the hf wave groups, and a perfect long wave absorption of reflected long waves at the wave paddle. However, this methodology can also be applied when an IFLW (spurious) is present. This extension of the array method was used in the present study to compute free spurious subharmonics in order to correct the wave generation. Once the wave generation is corrected, the wave signal at the group frequency is composed by the pair ILW-OFLW only. Hence, the separation is performed with the same starting conditions as in *Van Dongeren et al.* [2007]. A more detailed description of the used separation method is provided in *Padilla and Alsina* [2016].

2.3.2. Cross-Correlation Analysis and Wave Celerities

The matching degree between a pair of signals $V(t)$ and $Y(t)$ is quantified using a cross-correlation function, such as

$$R_{V,Y}(\Delta\tau)=\frac{E[V(t)Y(t+\Delta\tau)]}{(\sigma_V\sigma_Y)}, \tag{3}$$

where $E[\cdot]$ denotes the expected value and σ represents the standard deviation. The usual cross-correlation function $R_{V,Y}$ returns a value between -1 and 1, where 1 means a perfect match. This technique enables us to obtain the real propagation celerity *c* of any signal measured at consecutive wave gauge locations by computing the time lag $\Delta\tau$ between them. We apply this correlation technique to various combination of signals and therefore the notation of the correlation function varies depending of the pair of signals used. For instance, $R_{ILW,ILW}$ denotes the correlation function performed between pairs of ILWs. As in *Janssen et al.* [2003], the high spatial resolution of the measurement allows a representation of the cross-correlation functions in a quasi-continuous distribution in space.

2.3.3. Nonlinear Energy Transfers Based on HOS

The nonlinear wave interactions can be studied to the second order on the basis of high-order spectral (HOS) energy balance [*Hasselmann et al*., 1963; *Elgar and Guza*, 1985; *Herbers et al*., 2000; *de Bakker et al*., 2015, among others]. In these studies, the transport of energy associated with a frequency f is presented as a balance between the cross-shore gradient of the energy flux spectrum F_f, a nonlinear source $S_{nl,f}$ computed by bispectral analysis and a dissipation term $S_{ds,f}$ that includes energy losses such as wave breaking:

$$\frac{\partial F_f(x)}{\partial x} = S_{nl,f}(x) + S_{ds,f}(x). \tag{4}$$

We have followed this approach, neglecting directional spread of the waves and alongshore depth variations. Furthermore, using the separation procedure presented above, only incident waves will be considered for computing this nonlinear energy balance. From equation (4), $S_{ds,f}$ may be extended as a sink term that includes not just wave breaking losses, but any energy dissipation such as viscous dissipation along the flume. The cross-shore integration of equation (4) results in,

$$E_f(x) = \frac{1}{\rho\, g\, c_{g,f}(x)}\left(\rho\, g\, c_{g,f}(x_0) E_f(x_0) + \int_{x_0}^{x} \left(S_{nl,f}(x) + S_{ds,f}(x)\right) dx\right), \tag{5}$$

which assumes the linear approach that the spectral energy E travels with the wave group celerity c_g. Using the relationship between the spectral energy content and the wave height ($E = H^2/8$), the latter expression turns into:

$$H_f^2(x) = H_f^2(x_0)\frac{c_{g,f}(x_0)}{c_{g,f}(x)} + \left(\frac{8}{\rho\, g\, c_{g,f}(x)}\right)\int_{x_0}^{x} S_{nl,f}(x) dx + H_{ds,f}^2(x), \tag{6}$$

where the wave height grows due to shoaling (first term in the right-hand side of the equation) and nonlinear energy gains (second term). Conversely, $H_{ds,f}$ represents the height loss associated with the aforementioned sink term $S_{ds,f}$ where any dissipative processes may be included.

The nonlinear energy exchange term $S_{nl,f}$ is computed by integration of the imaginary part $\Im$ of the bispectrum for the desired frequency f:

$$S_{nl,f} = 3\pi\frac{\rho\, g\, f}{h}\Im\left\{\sum_{f'=0}^{f} B(f', f-f') - 2\sum_{f'=0}^{f} B(f', f)\right\}, \tag{7}$$

where the bispectrum B accounts for the phase coupling among triads of the frequency components [f_i, f_j, $f_i + f_j$]. It is formally defined as $B(f_i, f_j) = E[A_{f_i}^* A_{f_j}^* A_{f_i+f_j}]$, where A_f is the complex Fourier coefficient of the frequency f and the asterisk denotes a complex conjugate. Further details of the presented bispectral analysis can be found in *Padilla and Alsina* [2016].

In general, $H_{ds,f}^2(x)$ is a closure term since the incident wave amplitude H_f and the nonlinear energy balance $S_{nl,f}$ are known for every frequency. However, for the experimental wave conditions presented in this work, the sink term $S_{ds,f}$ has been defined as the time-averaged rate of energy dissipation due to bed friction [*Jonsson*, 1966]:

$$S_{ds,f} = \frac{2}{3\pi}\rho\, f_e\, (A\omega)^3, \tag{8}$$

where A and ω are the amplitude and angular frequency, respectively, and f_e is the energy dissipation factor set around 0.05 in smooth laminar conditions ($Re < 3\times10^5$).

2.3.4. Wave Asymmetry and Skewness Based on HOS

Skewness (Sk) and asymmetry (As) are geometric parameters that quantify the lack of symmetry to the horizontal and vertical axes, respectively. The skewness and asymmetry arising from second-order nonlinear wave coupling (also called wave-wave or triad interactions) can be evaluated from bispectrum analysis [*Elgar and Guza*, 1985]. Given a record of surface elevations η, the integral of the real and imaginary parts of the bispectrum B defines the skewness and asymmetry, respectively [*Hasselmann et al*., 1963; *Elgar and Guza*, 1985], i.e.,

$$Sk = \left[\int_{-\infty}^{+\infty}\int_{-\infty}^{+\infty} \Re\left\{B(f_i, f_j)\right\} df_i df_j\right] \Big/ E[\eta^2(t)]^{3/2}, \tag{9}$$

and

$$As=\left[\int_{-\infty}^{+\infty}\int_{-\infty}^{+\infty}\Im\{B(f_i,f_j)\}df_idf_j\right]/E[\eta^2(t)]^{3/2}, \tag{10}$$

where the normalizing factor $E[\eta^2(t)]^{3/2}=\sigma_\eta^3$.

3. Results

3.1. Breaking of the Incident hf Grouping Waves

The high spatial resolution of the present data enables a quasi-continuous tracking of individual wave crests in the spatial and temporal domain. In Figure 2a, a contour plot of the time and space distribution of the water surface elevation is illustrated. In the space-time domain, the trajectory, s, of an individual crest n (where n is the label of the wave crest) can be tracked by computing the propagation time of the crest n between wave sensors at known cross-shore locations. Therefore, the discrete trajectory of a high frequency wave crest n can be obtained from its celerity defined by

$$\frac{\mathrm{d}s(x_i,n)}{\mathrm{d}t}=\frac{\Delta x_i}{\Delta\tau_i}, \tag{11}$$

where Δx is the separation between wave sensors and $\Delta\tau$ is the time-lag computed using cross-correlation functions $R_{\eta,\eta}$ as described in section 2.3.2.

Figure 2a reveals the trajectories, s, of the different wave crests (colored lines) forming a wave group. By following the crest elevation along s, the wave crest breaking process and location are characterized accurately (accuracy of $\pm$0.05 m in the horizontal distance) as the maximum crest elevation within a trajectory in the nearshore areas. Since the short-wave breaking event takes place over the crests themselves, this process may only appear along the trajectory s for each constituent crest. In Figure 2a, the wave breaking location of individual waves is illustrated with circles. For the time being, it will be assumed that individual crests follow slightly parallel trajectories to each other, which means that the wave celerity is very similar for every single crest, as obtained from c_p, the phase celerity of the mean primary frequency. This assumption seems reasonable observing the trajectories depicted in Figure 2a and will be discussed later on.

The water surface elevation along individual crest trajectories s projected onto the axis x is presented in Figure 2c. The breaking location is clearly identified as the drastic decrease of the crest height as the wave crests propagate. The breaking excursion Δx_b is displayed as the shaded area in plot c. The distribution of the breaking events seems to follow a pattern given by the wave group modulation as illustrated also in plot a. However, analogous crests (same color) of the wave group break at remarkably different crest elevations depending on whether they are at the front or back of the group (although the crest elevation is initially the same). This breaking sequence is extended to the rest of the crests forming the groups and allows distinguishing between wave breaking at the frontside and the backside of the group. As can be seen in Figure 2c, the frontside (solid circles) always consists of higher breaking crests compared with the backside (open circles). This different breaking behavior is caused by the existence of long waves at the wave group frequency. Assuming a depth-induced breaking, the wave height to depth ratio γ offers a good description of the breaking sequence when the water depth is corrected with the measured low frequency amplitude. Figure 2d shows the wave height at breaking versus the effective depth $h^*(x,t)=h(x)+\bar{\eta}(x)+\eta_{lf}(x,t)$, where the still water depth h has been corrected with the mean water surface elevation, set down $\bar{\eta}$, and lf oscillations, η_{lf}. It is evident that this correction requires accurate time-space breaking identification, which does not present a problem due to the aforementioned dense resolution. For this specific case, *B-4*, the ILW dominates the lf signal and is out of phase, slightly lagging behind the hf wave group structure [*List*, 1992; *Janssen et al*., 2003; *Battjes et al*., 2004]. Therefore, it is responsible for larger breaking wave heights at the frontside of the wave groups. This phase lag will be investigated in detail in section 3.4. When the water depth at the breaking location is corrected with the lf waves, the wave height at breaking shows a linear distribution with the corrected water depth as illustrated by a dashed line in Figure 2d.

Figure 2b illustrates a set of time series at five fixed cross-shore locations across the surf zone. These time series illustrate the evolution of the wave groups from $x=7.43$ m, where no breaking is observed, to $x=3.23$ m, where the grouping modulation has been lost almost completely. The time evolution of the

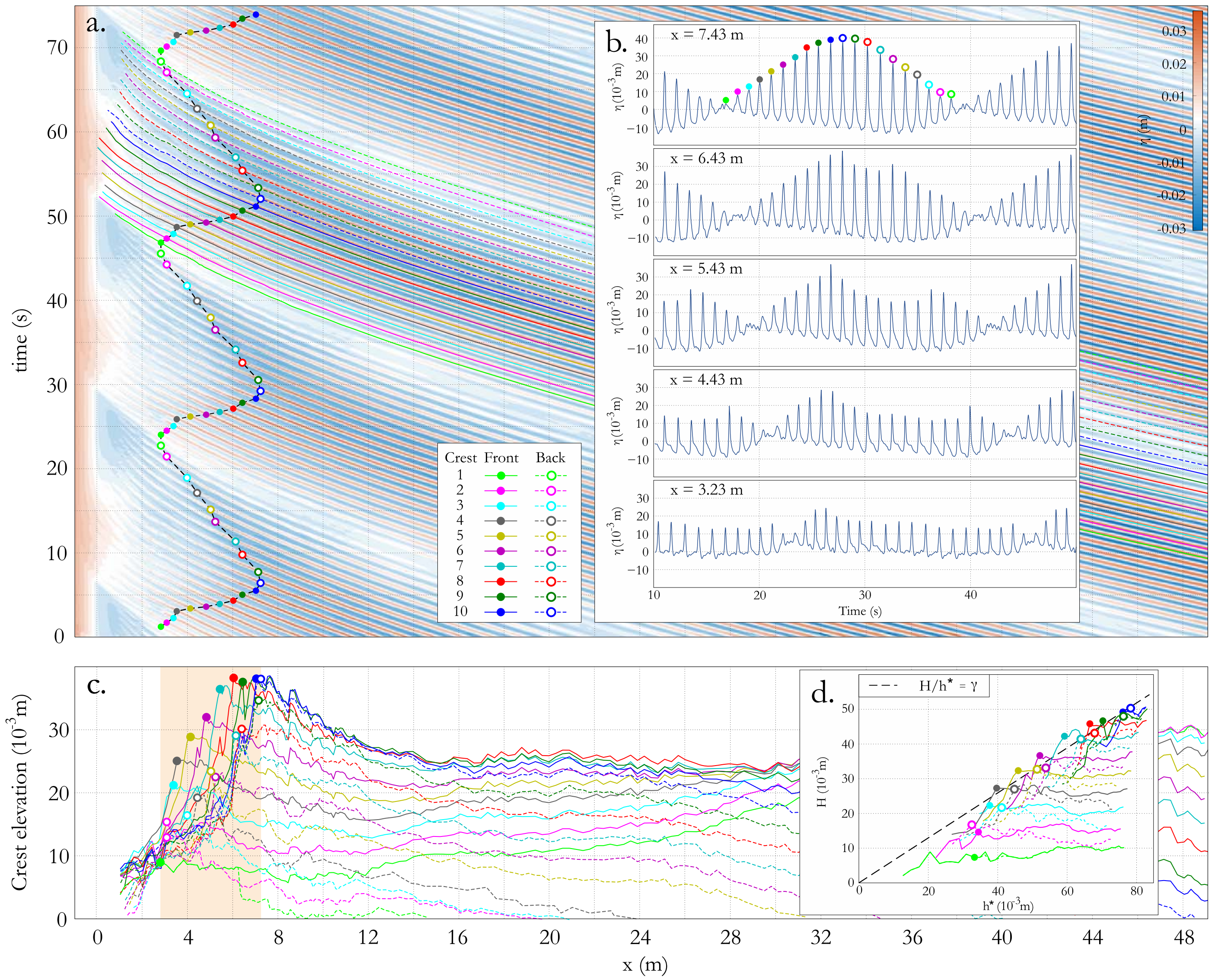

Figure 2. Contour plot of water surface elevation for case *B-4*. The individual wave crests as they propagate over the space-time plane are illustrated in plot a and the crest elevations (with respect to the mean water level) along the trajectories *s* are presented in plot c. The breaking location of individual waves is marked with colored circles. The shading zone in plot c represents the breaking excursion. Plot b includes the time series along the surf zone where the loss of wave group modulation is noticeable and plot d shows the wave height as $H = \eta_{crest} - \eta_{through}$ versus the actual water depth h^*.

varying breakpoint is already illustrated in Figure 2a (black dashed line with colored dots) where the waves at the frontside break earlier in time and at locations closer to the shoreline compared to similar waves at the backside. Likewise, Figure 2b shows the distribution of the individual waves breaking within the group. The breaking process starts in the center of the group, with the biggest waves, and the sequence moves to the adjacent ones at both sides, with a slight dominance for the backside where the effective depth is reduced due to the long wave presence. Across the surf zone, the wave group modulation is strongly reduced and the initial crest of the wave group turns into a flat sequence of bores that will eventually dissipate their energy close to the shoreline. The reduction in the wave groupiness due to the breaking of the largest waves is consistent with earliest observations of *Veeramony and Svendsen* [1996].

The same data treatment to identify individual hf wave breaking has been extended to all tested wave conditions. Figure 3 shows the differences in the spatial distribution of the breaking mechanism for hf waves within a wave group. For wave conditions *A* and *B*, wave breaking occurred predominantly at intermediate water, while for wave conditions *C* wave breaking occurred at intermediate and shallow water. Figure 3

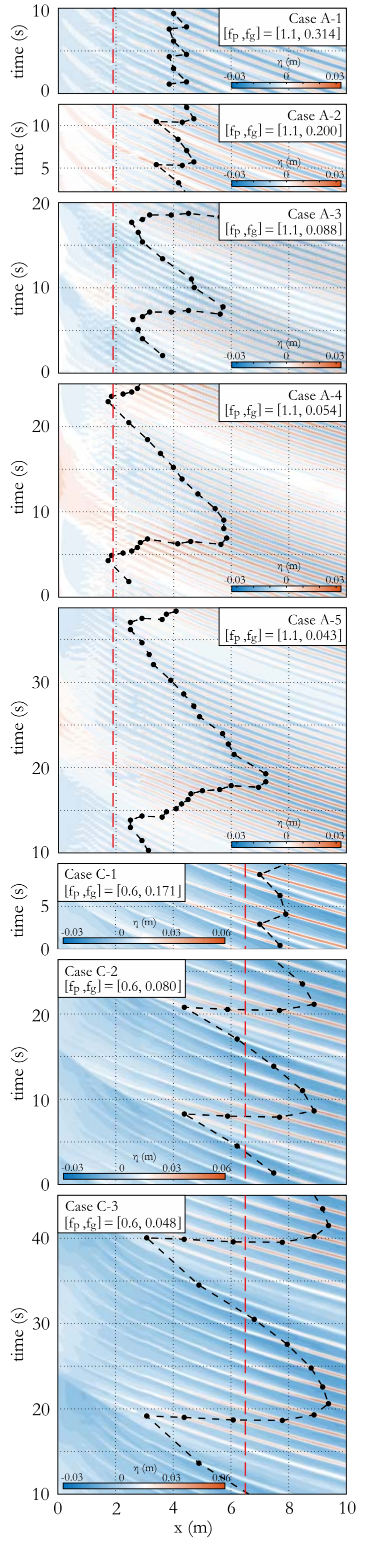

Figure 3. Space-time distribution of the varying breakpoint (black dashed line) for wave groups with $f_p=1.1$ Hz (plots a, b, c, d, and e) and $f_p=0.6$ Hz (plots f, g, and h). Black dots mark the locations of individual breaking events and the red dashed line indicates the shallow water limit x_{ShWL}.

shows that, for a given f_p value, the breaking onset (x_{ob}) moves seaward as the group frequency decreases. The highest waves (at the center of the group) break in deeper water whereas the smallest ones (at the edges of the group) travel further into shallower water, widening the surf zone. This is also translated into longer breaking cycles T_b since the breaking time modulation is inversely related to the grouping frequency ($T_b=1/f_g$). Therefore, with longer cycles and, consequently, higher number of constituent waves with the same mean period, the breakpoint excursion grows in time and space. For series *A*, the breaking onset moves from $x=4.45$ m to $x=7.20$ m for $f_g=0.314$ Hz, and 0.043 Hz, respectively, whereas, lower f_p-frequency wave conditions, series *C* ($f_p=0.6$ Hz), start breaking at $x=7.85$ m for $f_g=0.171$ Hz and move seaward to $x=9.38$ m as the group frequency reduces to $f_g=0.048$ Hz. Although smaller waves may break in shallow water, all these breaking onsets occur always before reaching the shallow water limit x_{ShWL} associated with the mean primary frequency (red dashed lines in Figure 3).

The wave height distribution of individual waves with respect to the actual water depth h^* has been computed for all the tested wave conditions (not shown) and indicates that the saturation law ($H=\gamma h^*$) describes the breaking sequence for every case remarkably well. The mean coefficient of determination R^2 is, in most of the tested cases, higher than 0.91 but with different γ values depending on f_p and group frequency. The influence of f_p on wave breaking is well known, with larger γ values for longer individual wave crests [*Bowen et al.*, 1968; *Battjes*, 1974; *Alsina and Baldock*, 2007]. The distribution of the observed γ values with the Iribarren number or similarity surf parameter ξ is presented in Figure 4a. There, the Iribarren number is computed close to the wave-maker as:

$$\xi_p=\frac{S}{\sqrt{H_s/L_p}}, \tag{12}$$

where S is the beach slope, L_p is the wavelength at the mean primary frequency (f_p), and H_s is the significant wave height computed from the standard deviation of the water surface signal. The γ is seen to increase for larger Iribarren numbers [*Bowen et al.*, 1968; *Battjes*, 1974] (Figure 4a, black dashed line). However, the scatter of the data is large, and for a given f_p value, it is also evident that there is an increase in the γ value as the group frequency increases. In other to retain the information of both influences, f_p and f_g, a modified Iribarren number is proposed, including the wave group structure:

$$\xi_p^*=\xi_p\left(\frac{L_p}{L_g}\right)^{\kappa}, \tag{13}$$

where L_g is the length of the group and κ is an empirical parameter that may depend on the beach slope. For practical purposes, $L_g\approx c_{gp}\cdot T_g$, assuming the linear theory group velocity of the primary waves at the mean primary wave frequency c_{gp} as a good approach of the group celerity (this

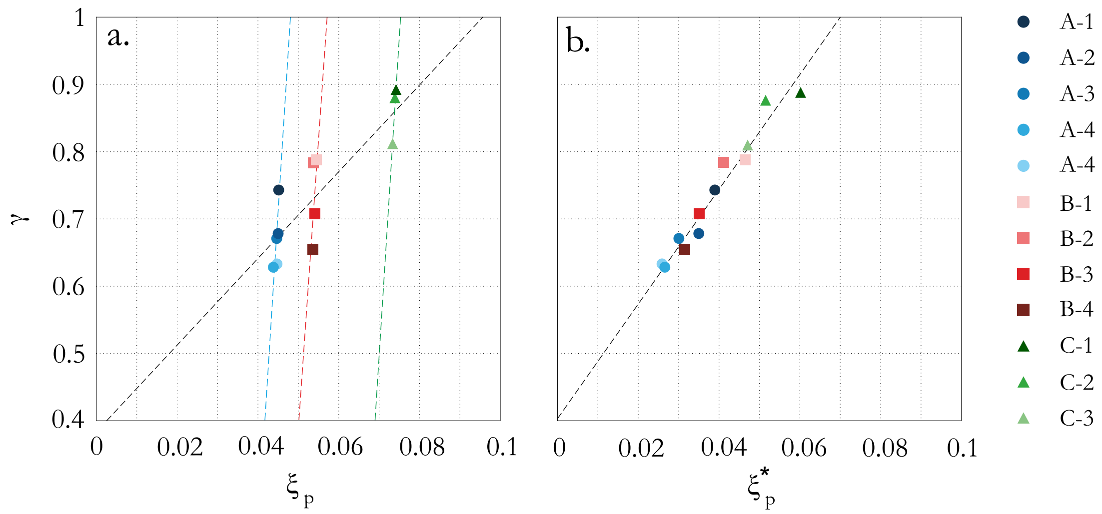

Figure 4. (a) Wave-height to effective-depth ratio (γ) in terms of the Iribarren number ξ_p. (b) The colored dashed lines illustrate the influence of the group frequency (f_g) in contrast to the influence of the hf waves (black). Both trends collapse onto a single one considering a modified Iribarren number ξ_p^* accounting for the grouping structure.

validation will be discussed later on in section 3.4). For a given value of κ=0.2, the modified Iribarren number presented in Figure 4b suggests a linear relationship $\gamma=8.52 \cdot \xi_p^*+0.4$, where wave conditions with a very different grouping structure (different grouping lengths and number of constituent crests), such as *B-1* and *C-3*, share a similar γ-value.

3.2. Skewness and Asymmetry of hf Waves

Although the saturation parameter, γ, describes the breaking process reasonably well, it does not offer a physical explanation of the wave group modulation (group frequency) influence on γ, or of the triggering of the wave breaking. Instead, the skewness *Sk* (a measure of the horizontal symmetry) associated to η_{hf} has been traditionally used to describe the wave breaking onset because of the wave shape instability [*Babanin et al.*, 2007].

Figure 5 shows the cross-shore distribution of the skewness and asymmetry for the tested wave conditions. The plots show an overall increase in absolute value of skewness and asymmetry during wave propagation consistent with previous reported measurements [*Doering and Bowen*, 1986, 1995; *Elgar and Guza*, 1985, 1986]. However, for a given f_p, a larger increase in skewness is observed as the group frequency decreases. At the same time, the onset of the asymmetry growth (in absolute value) is observed to move seaward as the group frequency decreases. A close relation between the maximum value in the cross-shore skewness

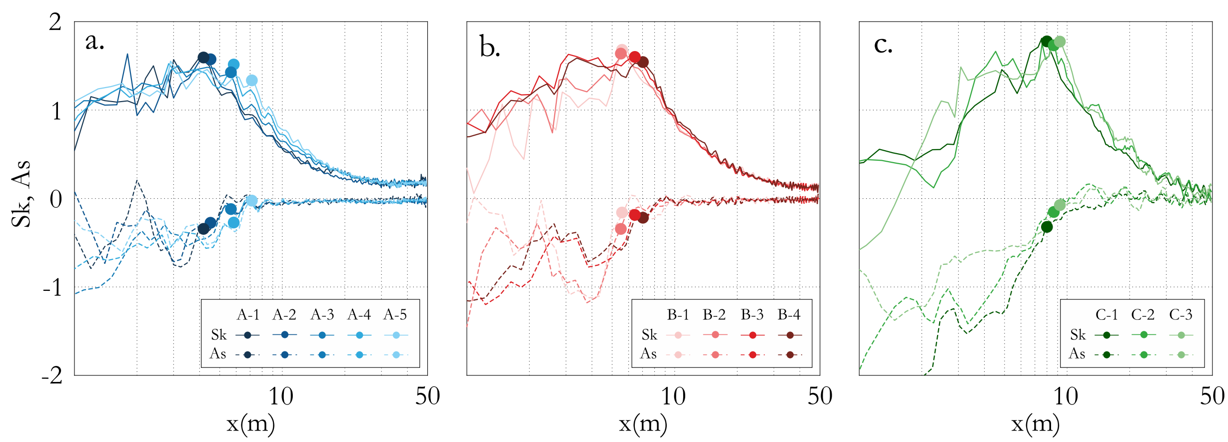

Figure 5. Cross-shore evolution of the hf wave skewness (solid line) and asymmetry (dashed line) for series (a) *A*, (b) *B*, and (c) *C*. The breaking onsets are displayed with dots.

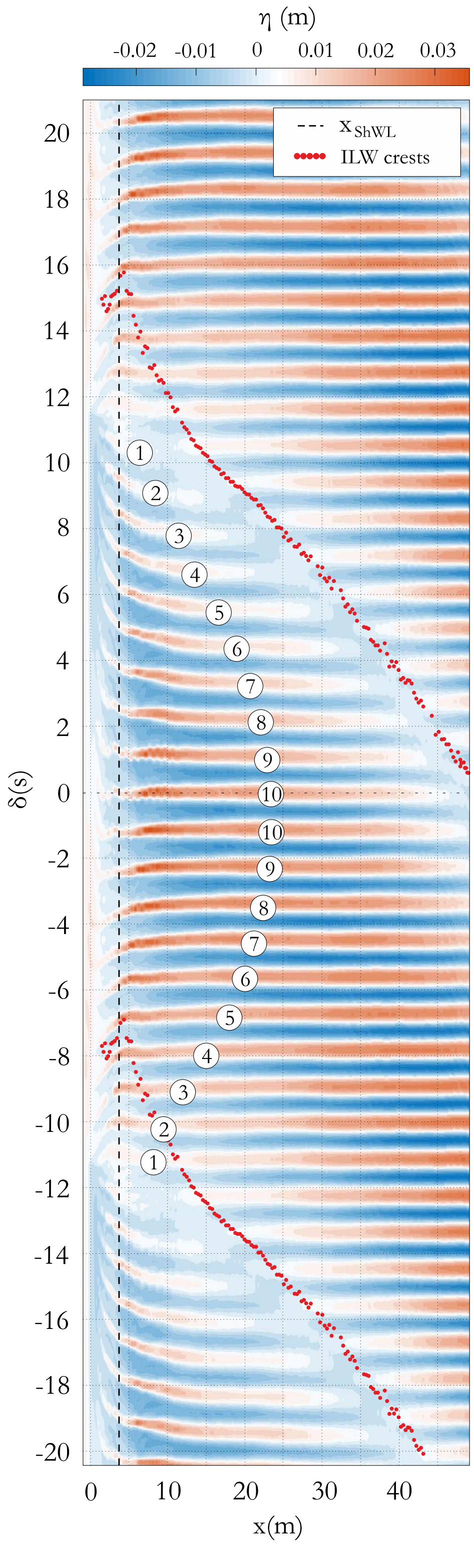

Figure 6. Contour plot of the surface elevation η in terms of the cross-shore location and time shift δ with respect to the central group crest 10. The black dashed line points out the shallow water limit for the mean primary frequency wave, whereas the red dots show the trajectories of the ILW crests.

distribution and the wave breaking onset is observed (Figure 5). During hf waves shoaling, the crest height grows larger than the trough depression, increasing wave skewness, and reaching a maximum ratio of around 1.5 before becoming unstable and breaking at x_{ob}. The breaking onset x_{ob} is obtained as the breaking location of the highest wave in the group as described in section 3.1. Trends in wave asymmetry/skewness are different for varying group frequencies, which is explained by the influence of the group frequency on the nonlinear energy transfer from the primary components to superharmonics and subharmonics. This link will be further discussed in section 4.

3.3. Wave Propagation Celerity

As mentioned above, the constituent wave crests follow parallel space-time trajectories *s* (Figure 2a), which implies the same propagation velocity. This is validated using the trajectory of a single wave crest as a reference to compare the relative time shift with the adjacent remaining crests. If the crests propagate with the same celerity, then the relative time shift among them must be a constant δ. In Figure 6, the water surface elevation contour plot is displayed with respect to the cross-shore location and time shift between individual waves and the selected reference wave crest, which is the wave crest $n=10$ at $\delta=0$. The remaining crests are straight lines (δ=*const*) until they approach the shallow water limit (black dashed line). As the individual waves travel to shallow water depths, where the propagation celerity depends on the water depth, the back-sided crests (top half in Figure 6) slow down, increasing the time shift (positive δ) with respect to the reference wave due to the presence of lower water depth induced by the low frequency wave trough, η_{lf}, whereas the waves in the frontside (bottom half) speed up travelling on locally deeper areas around the ILW crest (red dots). These differences in individual wave celerity in shallow water caused by the variations in water depth and velocity induced by long waves have already been observed by *Tissier et al*. [2015]. The intrawave variability of celerity can modify the wave-field considerably in shallow water inducing bore "focusing" or "merging" as illustrated by *Sénéchal et al*. [2011] (i.e., faster bores overtake slower bores and focusing) and will be discussed further in section 3.6. Figure 6 shows that intrawave variability in celerity is low before reaching shallow water suggesting that most of the wave celerity differences are induced by the water depth variations caused by the long wave presence, which grows with decreasing water depth. This influence seems larger than any wave celerity variability induced by differences in wave height or amplitude-dispersion [*Thornton and Guza*, 1982].

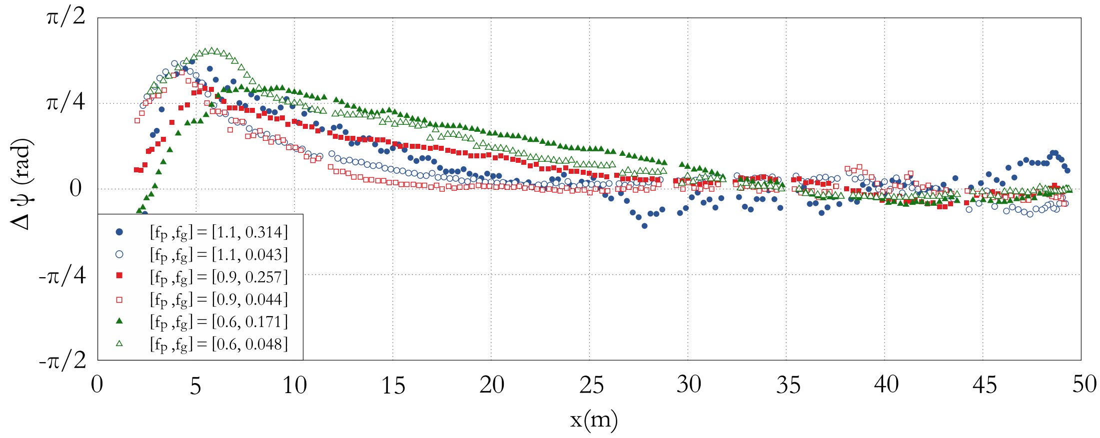

Figure 7. Additional phase shift $\Delta\psi$ between the group structure and the ILW, above the expected π-shifted phase typical from the equilibrium solution. ILWs lag behind the groups for positive values of $\Delta\psi$. The present cases show the longest and shortest groups for series *A* (blue circles), *B* (red squares), and *C* (green triangles).

3.4. Phase Lag of the lf Waves

The dynamics of the lf motions associated with the wave groups will be illustrated in this section. The ILW celerity has been computed by the cross-correlation functions $R_{ILW,ILW}$. A growing propagation time-lag is observed between τ_{ILW} (the cumulative propagation time of the ILW) and τ_{gp} (the theoretical propagation time associated with the group structure), where the ILW lags behind the groups as they propagate to shallower water. The relative phase shift ψ between ILW and the wave group structure is obtained as $\psi=\pi+2\pi f_g(\tau_{ILW}-\tau_{gp})$, and the additional phase shift with respect to the theoretical π value as $\Delta\psi=\psi-\pi$. Figure 7 shows the cross-shore variation of the additional phase shift $\Delta\psi$. Close to the wave-maker, where an equilibrium situation is expected, $\psi \approx \pi$ which means that the ILW and the group structure are in antiphase. After hf wave breaking and when approaching shallow water depths, the additional phase shift decays. This may be due to nonlinearities in this region which also affect the separation method. More importantly, during hf wave shoaling, ψ separates from π strongly as the group frequency decreases.

3.5. Nonlinear Energy Transfer

Nonlinear energy transfer between harmonics will be examined using a higher-order spectral technique accounting for triad interactions. The shortest (*C-1*) and longest (*C-3*) wave group modulation of series *C* will be analyzed. Similar behavior was observed for series *A* and *B* but series *C* showed more energetic low frequency components which helped to better explain the observed behavior. Figures 8 and 9 gather the spatial evolution of the high and low frequency components for wave conditions *C-1* ($[f_1,f_2]$ = [0.686 Hz, 0.514 Hz]) and *C-3* ($[f_1,f_2]$ = [0.624 Hz, 0.576 Hz]), respectively. Plot *a*, in both cases, shows a contour plot of the cross-shore and frequency spectral distribution. Initially, close to the wave paddle, the spectral energy is dominated by the target primary frequencies (f_1 and f_2), around f_p=0.6 Hz. During wave group propagation, high and low frequency components arise as a consequence of triad interactions. Whereas superharmonics grow quickly during hf wave shoaling, they also dissipate during hf wave breaking (dashed black line denotes the breaking onset). After hf wave breaking, the remaining energy is dominated by subharmonic components. The energetic growth of these higher-order components may be noticeable up to the third order for some cases [*Johannessen and Swan*, 2003], but in this work we mainly focus on nonlinear interactions up to the second order (sum-interaction, difference-interaction, and self-interaction terms).

Plots *b* and *c* present the cross-shore amplitude evolution for the high and low frequency components, respectively, comparing them to the evolution of the primary components, f_1 and f_2. In the vicinity of the wave-maker, the primary components concentrate more than 98% of the spectral energy content, which progressively decreases as they travel shoreward and transmit energy to higher and lower frequency components. Both plots display the measured amplitudes at different frequency components (Md) and the computed ones (Cp) based on equation (6). Furthermore, the ingoing and outgoing amplitude obtained from the separation procedure (Sp) at f_g (ILW and OFLW) are also shown, where the separated OFLW is compared

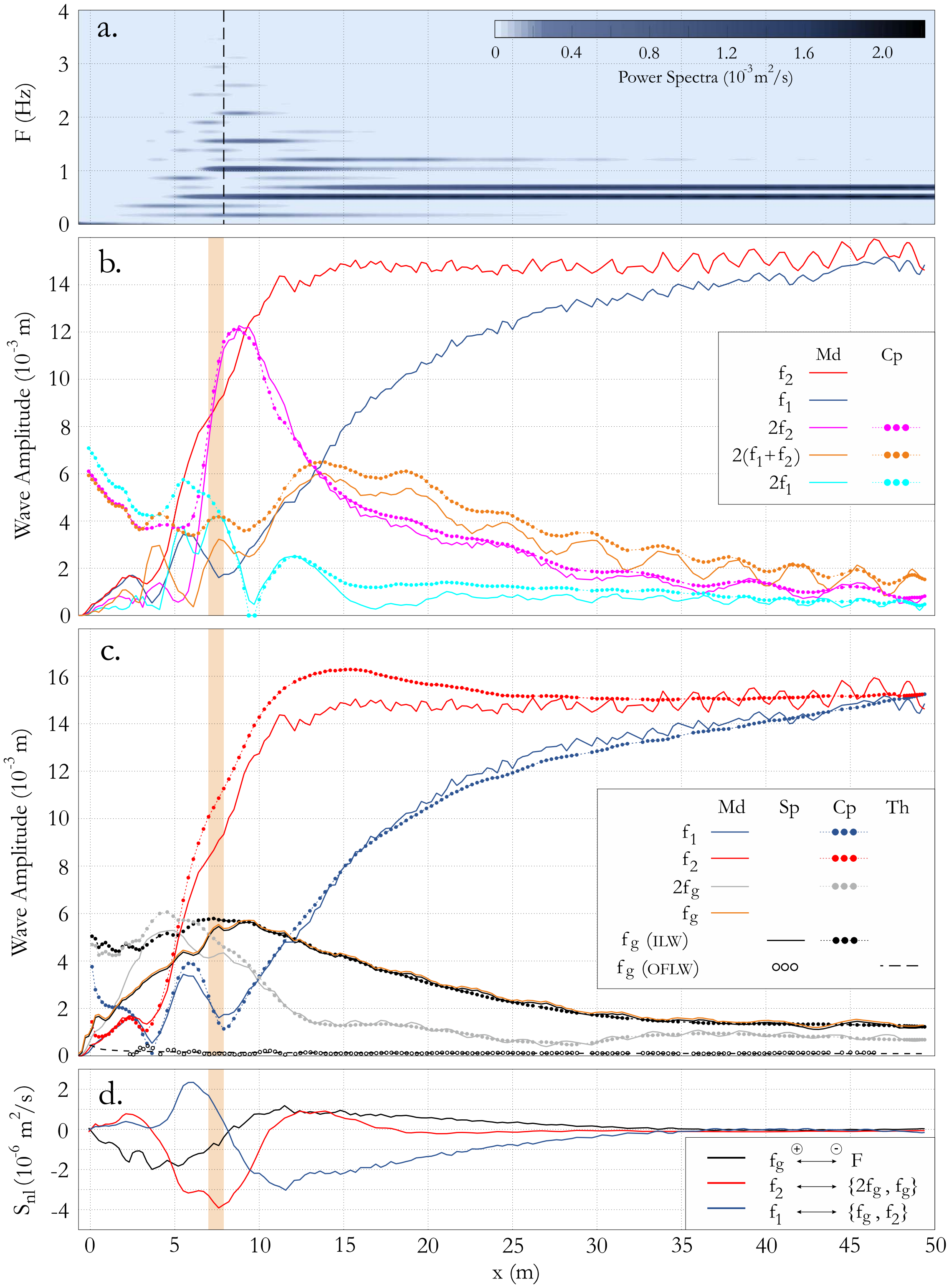

Figure 8. Plot a shows the cross-shore distribution of power spectra density at different frequency components for the case *C-1* ($[f_1,f_2]$ = [0.686 Hz, 0.514 Hz]). The black dashed line denotes the breaking onset. Plots b and c gather the cross-shore amplitude evolution of components belonging to the high and low frequency domain, respectively. Therefore, the amplitudes measured from the data (Md) are compared to the computed (Cp), separated (Sp), and theoretical (Th) ones. Finally, plot d presents the energy fluxes to(+)/from(−) the primary waves from(−)/to(+) the rest of their triads; and to(+)/from(−) the ILW from(−)/to(+) the rest of the frequency domain *F*. The brown shaded region represents the breakpoint excursion. β_b=0.104 for this case.

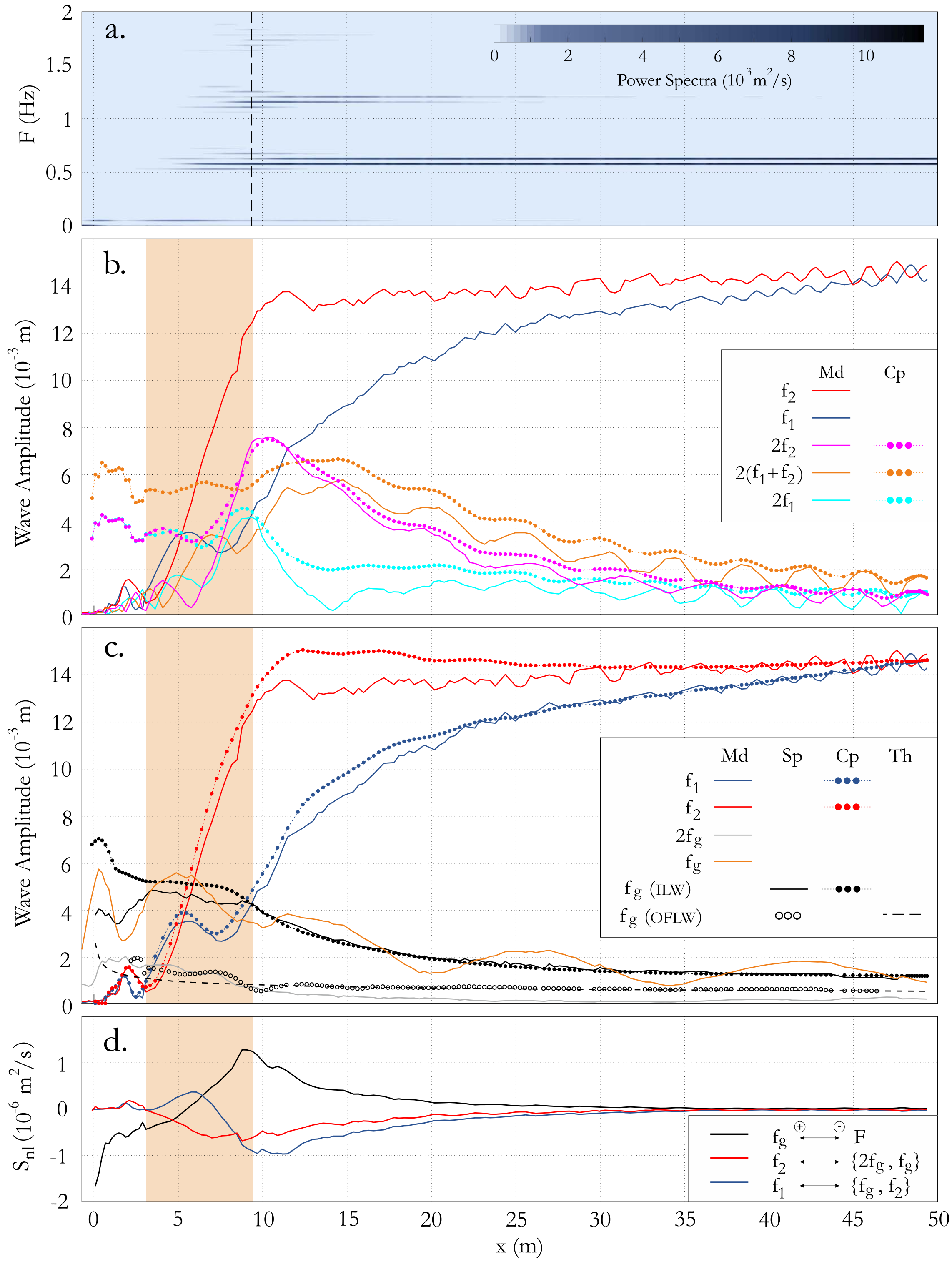

Figure 9. Plot a shows the cross-shore distribution of power spectra density at different frequency components for the case *C-3* ([f_1,f_2] = [0.624 Hz, 0.576 Hz]). The black dashed line denotes the breaking onset. Plots b and *c* gather the cross-shore amplitude evolution of components belonging to the high and low frequency domain, respectively. Therefore, the amplitudes measured from the data (Md) are compared to the computed (Cp), separated (Sp), and theoretical (Th) ones. Finally, plot d presents the energy fluxes to(+)/from(−) the primary waves from(−)/to(+) the rest of their triads; and to(+)/from(−) the ILW from(−)/to(+) the rest of the frequency domain *F*. The brown shaded region represents the breakpoint excursion. β_b=0.339 for this case.

to its linear theory cross-shore evolution (Th). No dissipation term ($H_{ds,f} \approx 0$) has been considered for computing any component but for the primary ones (f_1 and f_2) only.

Overall, the second-order components are well explained in terms of nonlinear triad-interaction energy exchanges until the wave breaking onset. For the wave condition with the larger group frequency (*C-1*) and within the hf domain (Figure 8b), the higher growth is in general observed by the self-self interaction component of f_2 ($\{f_2, f_2\} \rightarrow 2f_2$), whose maximum is reached just before the wave breaking onset. At the same time, the energy budget associated with $2f_1$ remains remarkably low compared to $2f_2$, whereas the sum term $2(f_1+f_2)$ reaches its maximum amplitude far outside the surf zone. Likewise, in the lf domain (Figure 8c), the ILW grows considerably during hf wave group shoaling, reaching a maximum energy content at the onset of the hf wave breaking (Figure 8c) where the shallow water limit is not reached yet. After hf wave breaking, the lf amplitude reduces but other lf components ($2f_g$) still grows. Shoreward $x \approx 5$ m the ILW and $2f_g$ component reduces considerably to reach an almost zero amplitude at the shoreline. This reduction in lf amplitude close to the shoreline is not explained by nonlinear frequency interactions (see Figure 8c separated Sp and computed Cp).

The nonlinear energy flux attributed to each component is illustrated in Figure 8d. This energy contribution varies during propagation and depends on the involved frequency components. Therefore, positives fluxes mean that f_g, f_1, and f_2 receive energy, whereas negative ones imply a transfer of energy from those to the rest of the triad. Particularly, the balance over f_g accounts for the resultant balance throughout all the triad interactions where f_g is involved (this is simplified in the legend as the whole frequency domain *F*). In fact, it may be seen that the f_1 component is the main energy supplier and responsible for the ILW enhancement (blue line in Figure 8d). According to that, the maximum ILW amplitude is reached at the same place where f_1 transfers its highest energy content. The differential transfer of energy from the primary frequencies to the lf domain illustrates the selective loss of energy for f_1 compared to f_2 as previously reported by *Baldock et al*. [2000] and *Alsina et al*. [2016].

The wave condition (*C-3*), illustrated in Figure 9, is characterized by a lower group frequency (longer wave groups) than *C-1* (Figure 8). There are small differences in the growth of the $2(f_1+f_2)$ component which presents a maximum close to the surf zone, a slightly smaller growth of $2f_2$ and also slightly larger growth of $2f_1$ for the case with the lower group frequency *C-3*. However, the most distinguishing feature is a considerable smaller decay of the f_1 component (f_2 also shows a slightly smaller decay). In the low frequency domain, a smaller growth of the ILW is observed in Figure 9c consistent with the smaller decay of f_1. The ILW does not reach a clear maximum at the breaking locations as for case *C-1* but increases slightly in amplitude across the breaking region and reduces in amplitude after the breaking location of the smallest hf waves indicating the loss of the group modulation. Also for *C-3*, the maximum combined $[f_1, f_2]$ contribution is again reached at the breaking onset but after that, they still supply energy with a lower rate which explains a gentle ILW growth along the surf zone. In general, throughout the studied cases, the breaking onset is an inflection point in the ILW growth due to the dissipation of primary components by hf wave breaking. Within the surf zone, the ILW may either keep growing with a lower rate for larger wave group periods or just decrease for smaller wave group periods.

The overall behavior of high and low frequency components during wave group propagation is summarized in Figure 10 for all tested wave conditions. The cross-shore distribution of the maximum hf wave envelope (top figures) and the absolute growth of the ILW (bottom figures) are illustrated for wave series *A* in Figures 10a and 10d, *B* in Figures 10b and 10e; and *C* in Figures 10c and 10f. The absolute growth is expressed as the ILW height (H_{ILW}) difference at any cross-shore location with respect to the initial one (H_{ILW,x_0}) close to the wave paddle. H_{ILW,x_0} is provided in Figure 11a compared with the equilibrium solution $\tilde{H}_{ILW}$ over a flat bed proposed by *Longuet-Higgins and Stewart* [1962]. This comparison is achieved 3 m away from the wave paddle, in the deepest region where a flat bottom is deployed along 1.5 m. Other authors such as *Baldock et al*. [2000] or *Alsina et al*. [2016] have validated this second-order solution with a satisfactory fit around $\varepsilon = H_{ILW}/\tilde{H}_{ILW} \approx 1$. However, for our simulations, since this flat bottom length represents between 7% and 50% of the running ILW wavelength for the longest and shortest groups, respectively, the equilibrium second-order solution may not be fully developed. Consequently, the theoretical solution underestimates the energy at the group frequency by approximately 33%, or alternatively, ε raises to 1.5.

For a given mean primary frequency f_p, the hf wave envelope maxima show (Figure 10) a larger growth as the group frequency decreases (increasing wave groups length) consistent with the larger growth of wave

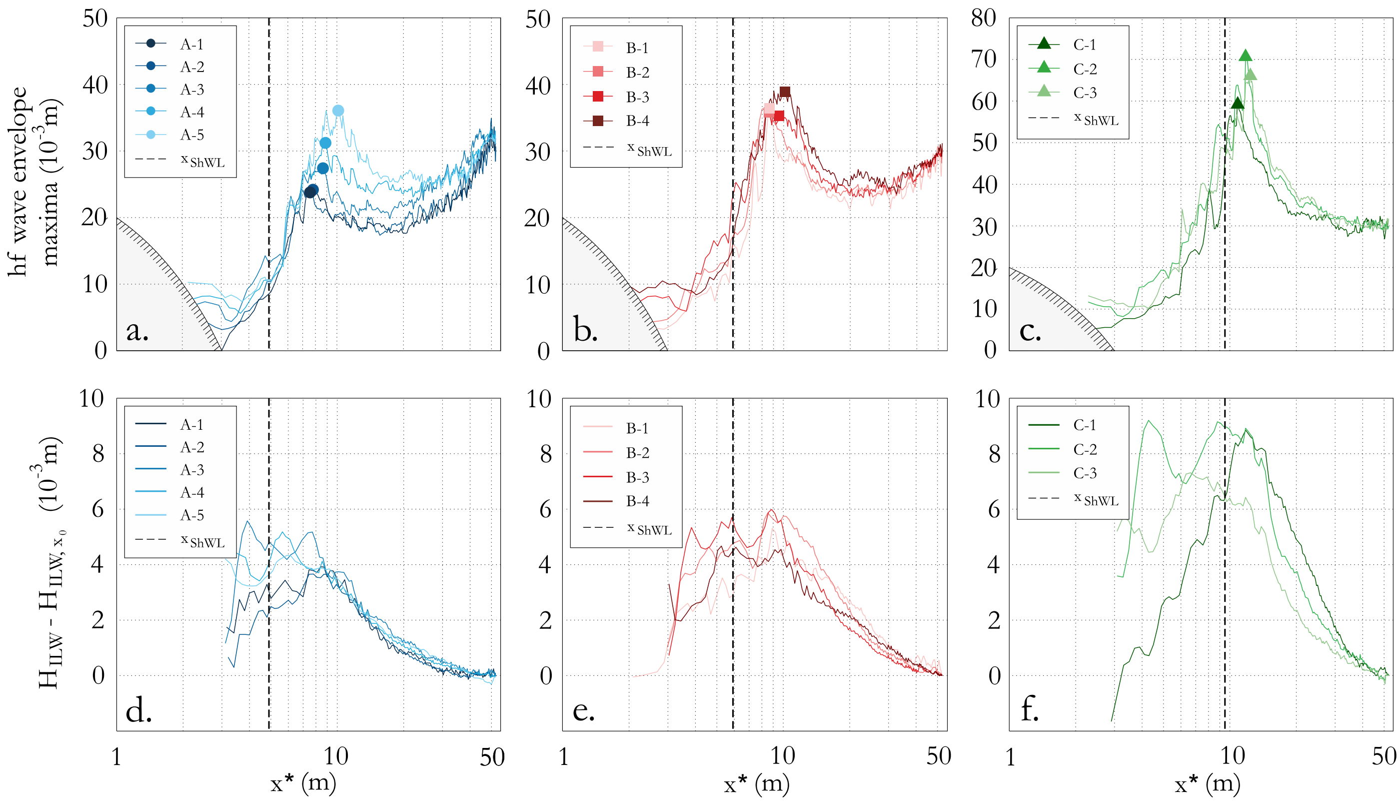

Figure 10. Cross-shore distribution of the (top plots) hf wave envelope maxima and (bottom plots) ILW height growth. The dots mark the breaking onsets for each wave case, whereas the black dashed line indicates where the shallow water limit is reached. The spatial domain has been plotted in log-scale to enhance the surf-swash region and has also been modified as $x^* = x + 3$ to include swash areas beyond the shoreline.

asymmetry and skewness illustrated in Figure 5 and, thereby, producing a breaking onset in larger water depths. On the contrary, the ILW behavior shows a larger wave height growth up to the breaking onset as the group frequency increases. This is consistent with the increasing phase-lag between the wave group structure and the ILW for increasing group frequencies as shown in Figure 7. After the onset of hf wave breaking, an important ILW height decay is observed for high group frequency conditions (short-wave groups, see cases *A-1*, *A-2*, *B-1*, *B-2*, and *C-1*). For these wave conditions, the wave group modulation is lost over a narrow breaking region due to the small breaking excursion induced by the group modulation. The long wave amplitude at the shoreline is minimal for these wave conditions. However, for wave conditions

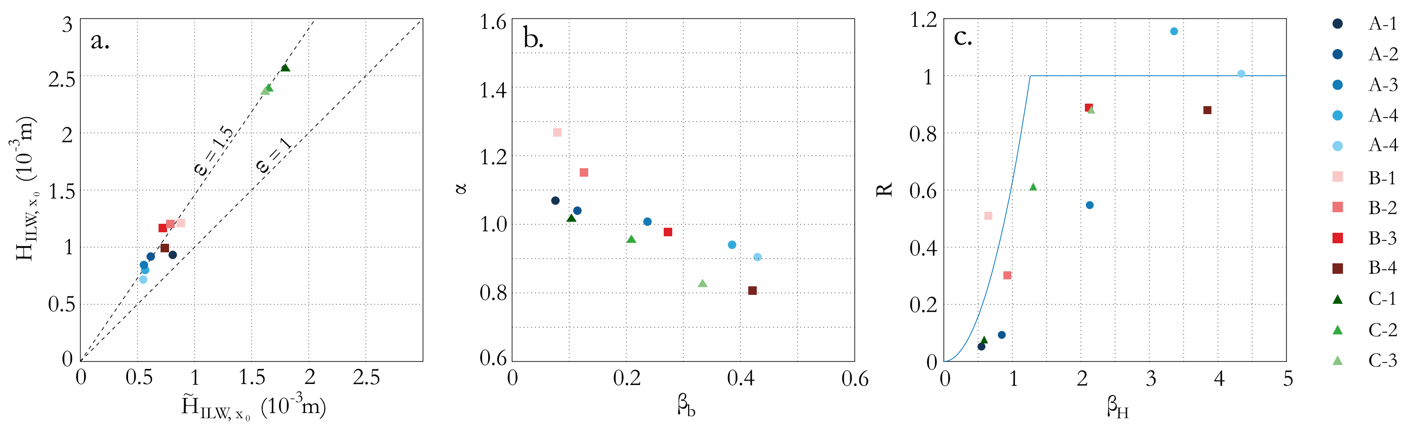

Figure 11. Plot a compares the initial measured ILW height (H_{ILW,x_0}) with the equilibrium solution ($\tilde{H}_{ILW,x_0}$), close to the wave-maker. Plot b gathers the ILW growth rate during hf wave shoaling (α) as a function of the normalized bed parameter β_b. Plot c presents the reflection rate R of the ILWs in the nearshore areas in terms of β_H.

with low group frequency (long wave groups), the ILW demonstrates a limited growth after the hf breaking, associated to a larger breaking area, a progressive reduction in the wave group modulation, and the progressive reduction in the primary waves contribution to the group frequency shown in Figure 11c. The location of ILW dissipation does not coincide with the onset of hf breaking, but rather occurs close to the shoreline, after the breaking of the smallest hf waves in the group.

The ILW behavior as it travels with the incident hf wave groups is presented in Figure 11. *Van Dongeren et al.* [2007] evaluated the growth rate of the ILW by fitting a function of local depth with an unknown power α of the water depth, as $H_{ILW} \propto h^{-\alpha}$, using experimental data and numerical simulations. They observed this value of α always to be below 2.5, defined as the maximum theoretical "shoaling" law for bound waves over a sloping bottom, and above 0.25 (Green's law), typical for free waves during shoaling. Overall, our data confirms that the ILW height growth increases with the group frequency for the gentle slope tested in the present experiments (Figure 11b). Extending this finding to a larger range of wave group frequencies, the results agree with the α values presented by *Van Dongeren et al.* [2007], where the growth rate becomes weaker for increasing β_b.

3.6. Low-Frequency Energy Dissipation After High Frequency Wave Breaking

From Figures 8 and 9 (plot *c*) and Figure 10, the ILW energy is observed to decay strongly in the nearshore areas for the wave conditions with higher group frequency, whereas for the cases with lower group frequency, a remarkable percentage of the ILW energy is conserved and reflects at the shore to travel seaward as an Outgoing Free Long Wave (OFLW). Consequently, the reflected waves (OFLWs) are more energetic as the group frequency decreases since the amplitude of the ILW and OFLW is very similar around $x = 0$ (Figure 9c). As the definition of the reflection coefficient R is influenced by the location at which it is defined, being influenced by both the varying incoming and outgoing components, in this work, we have defined a more convenient variable D. This accounts for the ratio of ILW dissipation across the surf zone and reflection at the shoreline as:

$$D = \Delta H_{ILW} / H_{ILW,x_{ob}}, \tag{14}$$

where ΔH_{ILW} is the difference between H_{ILW} at the breaking onset x_{ob} and H_{ILW} at the shoreline. This variable may be easily related to the reflection coefficient used in previous works [*Battjes et al.*, 2004; *Van Dongeren et al.*, 2007; *de Bakker et al.*, 2014] as $D = 1 - R$. Accordingly, similar results are achieved in Figure 11c compared to the presented ones in *Van Dongeren et al.* [2007]. Plot c gathers the reflection coefficient for the tested cases compared to the nondimensional parameter β_H in deep water that accounts for the steepness of the beach (slope) relative to the initial steepness of the ILW. Figure 11c confirms that shorter groups (groups with the lower number of constituent crests) undergo a lower reflection, or alternatively, higher lf dissipation across the surf zone. The reflection coefficient is almost null ($R \approx 0$) for the cases with higher group frequency and increases to about 1 for those with lower group frequency. The data tends to follow the relation between the reflection coefficient and the surf similarity parameter $R = 0.1\xi^2$, found by *Battjes* [1974] and plotted in solid blue line. Actually, our data agrees with *Battjes* [1974] and *Van Dongeren et al.* [2007] yielding a transition point at $\beta_H \approx 1.25$, where dissipation is no longer expected for longer groups.

The analysis of the lf energy dissipation close to the shoreline for wave conditions with higher group frequency shows a growing importance of the self-self interaction of the wave group frequency component (see Figure 8c). For the case *C-1*, the component $2f_g$ exhibits a larger energy growth of around 3 times higher than in case *C-3*. When the group is composed of three short waves only, it is observed that $2f_g = f_2 - f_g$. This implies that $2f_g$ is at the same time a superharmonic of f_g and subharmonic of the triad interaction composed by f_2, f_g. Therefore, its energy gain is larger. This statement may be analytically proven using the definition of f_2 in terms of the group frequency, f_g:

$$f_2 = f_p - f_g/2, \tag{15}$$

and using equation (2) to replace $f_p = f_g\,(n + 1/2)$. As a result,

$$f_2 = n \cdot f_g, \tag{16}$$

and particularly for $n = 3$, $f_2 = 2f_g + f_g$. In Figure 8c, (*C-1*) can be observed that the amplitudes of f_g (black) and $2f_g$ (grey) reach a similar maximum value, which is not the case for *C-3* (Figure 9c). *Van Dongeren et al.*

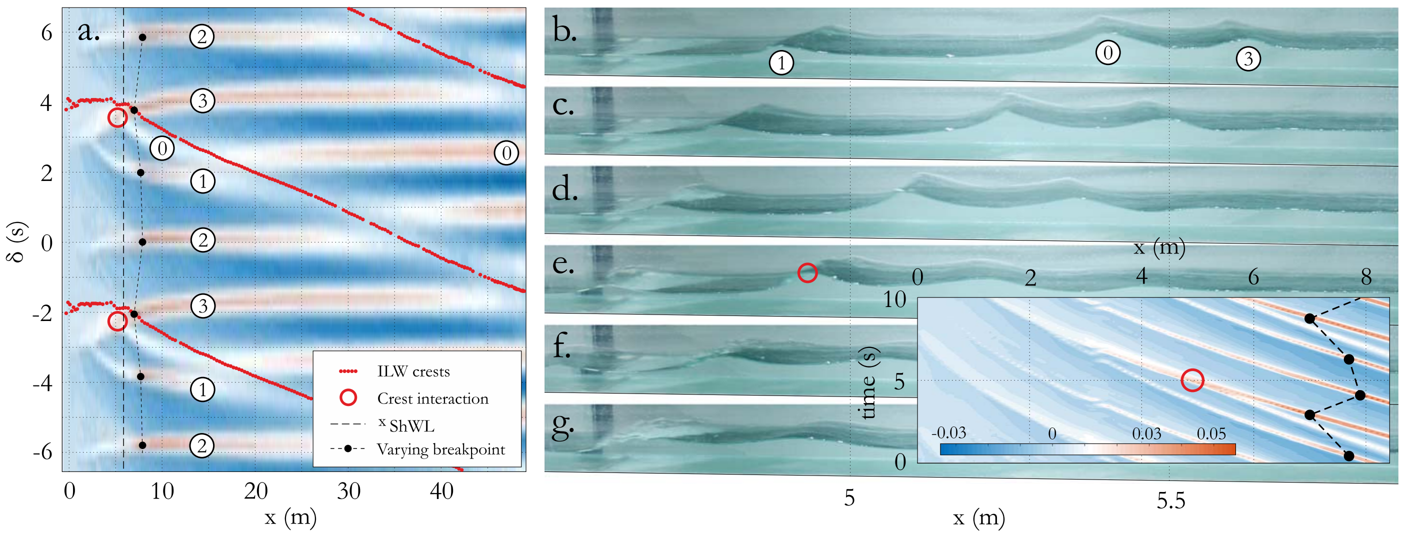

Figure 12. Identification of the additional breaking event (red circle) not belonging to the varying crest-breaking points (black dots) for the case *C-1*. Plot a shows the water surface elevation contour plot in terms of the relative time delay δ among crests, where the wave convergence in the limit between consecutive groups is evident. The wave belonging to the front side of the group (3) speeds up chasing (0) in the surroundings of the ILW crest (red dots). Plots b–g present the sequence of lab-pictures that record the process.

[2007] roughly mentioned the importance of f_2-f_g in the lee side of lf waves. With the present data, the fact that $2f_g=f_2-f_g$ shows a direct implication of the interaction between primary wave components and lf components in the increasing lf wave steepness, such that, this ILW becomes unstable and eventually break as *Van Dongeren et al*. [2007] suggested.

For case *C-1*, Figure 12 presents the water surface contour plot distribution with the cross-shore location and time-lag with respect to a central grouping crest $n=2$ and an isolated lf wave breaking event (at the red circle). This wave condition is initially characterized by 3–4 individual waves per wave group. The wave crest $n=3$ travelling nearly at the crest of the lf motion when arriving to shallow water conditions is shown to speed up while wave crests $n=0$ and $n=1$, travelling with the trough of the lf motion are shown to slow down. Wave crest $n=3$ reaches wave crest $n=0$ at the red circle marked location, focusing in the vicinity of the crest of lf components (*ILW* and $2f_g$). As a result, an isolated lf wave breaking event is illustrated at the area marked with a red circle at approximately $x=5.5$ m. The sequence *b–g* shows the individual wave crests while focusing. Immediately after, the lf wave is shown to break (Figure 12g). This latter lf breaking point is consistent with the $2f_g$ decay after reaching a maximum around $x=5$ m as illustrated in Figure 8c.

4. Discussion

Nonlinear energy transfer between frequency components in the form of second-order triad interactions causes the growth of both superharmonics and subharmonics of the primary components. In the hf domain, the group frequency has been shown to influence the behavior of the primary components and their superharmonics.

In the shoaling zone, the wave groups with low group frequency experience a slightly larger growth of their superharmonics ($2f_1,\ f_1+f_2$) compared to wave groups with high group frequency, and more importantly, a smaller dissipation of the primary frequency components, in particular f_1. This trend, a reduced decay of f_1 for decreasing group frequency, has already been reported by previous authors [*Baldock et al*., 2000; *Alsina et al*., 2016] and may only be attributed to nonlinear transfers of energy to superharmonics (i.e., $2f_1,\ 2(f_1+f_2)$) and lf components (f_g). As the groups travel shoreward, it is difficult to assess which frequency component contributes more to the wave skewness since the wave shape is the result of the contribution of all the harmonics and superharmonics. Nevertheless, it is clear from the present experiments that the group frequency f_g results in a good descriptor of these nonlinear exchanges of energy and their further implications in hf wave skewness and eventual breaking. A clear tendency of low group frequency wave conditions to promote a larger growth in the wave skewness has been observed, whose immediate consequence is an earlier breaking onset. The presented results are consistent with previous analysis of random wave conditions [*Norheim et al.*, 1998; *Rocha et al.*, 2017] showing an increase in hf wave asymmetry when the spectral bandwidth is narrowed (which leads to longer wave groups). *Norheim et al.* [1998] attributed this to the fact that sum and difference interactions tend to cancel in broad spectrum conditions. The group frequency controls the group modulation and the nonlinear energy transfer to superharmonics ($2f_1,\ 2f_2,\ f_1+f_2,\ldots$) that contributes to the wave asymmetry. Moreover, the group frequency also influences the energy transfer to low frequency components and the consequent decay of primary components also affecting to the wave asymmetry. The present data show that a larger growth of lf waves (i.e., ILW) is accompanied by a loss of horizontal hf wave asymmetry or amplitude. Previous works [*Baldock*, 2012; *Alsina et al.*, 2016] have already suggested this link between high and low frequency energies. The influence of the wave group modulation in wave skewness and breaking has important implications in coastal morphology as shown in *Alsina et al.* [2016]. Therefore, long wave groups (low group frequency) induced earlier wave breaking and a breaker bar located at further seaward locations. A modification of the Iribarren number, equation (13), has been proposed to account for the influence of the wave group modulation on the hf wave breaking parameter γ. However, the applicability of equation (13) to random wave conditions where wave group modulation occurs over a wide range of group periods requires further investigation.

In the lf domain, the presented influence of the wave group frequency on the growth of the ILW (which travels bound to the group structure before hf wave breaking) is consistent with previous works [*Battjes et al.*, 2004; *Van Dongeren et al.*, 2007], showing a clear growth dependence on the parameter β_b when the primary wave forcing is nonresonant (as in the present study). Based on the present work, f_1 is in general the main energy supplier to f_g. Therefore, a larger decay of f_1 for large group frequency wave conditions (low values of β_b) is likely to have a larger contribution to the growth of the ILW. Since the ILW growth and its time-lag behind the hf wave structure are physically related, the influence of the group frequency on $\Delta\psi$ has been illustrated. Increasing the difference frequency (decreasing β_b for the given beach slope) results in larger phase lags, consequently associated to a larger ILW enhancement. With the present data, the varying breakpoint generation [*Symonds et al.*, 1982; *Symonds and Bowen*, 1984] was not observed. *Baldock et al.* [2000] suggested that the breakpoint mechanism becomes ineffective when the breakpoint excursion Δx_b becomes larger than a certain fraction (0.2–0.3) of the long-wave wavelength. This was always the case for the present experimental conditions (not shown).

In the surf zone, hf wave modulation is reduced due to short-wave breaking and, therefore, the primary wave forcing is reduced. For wave cases of low group frequency (long groups), this results in only a slight reduction in lf wave amplitude as a consequence of, both, the progressive reduction of the forcing from primary waves components, and nonlinear energy transfer from the group frequency to hf components. The remaining lf energy is reflected at the shore and a fairly good correlation between the incident and outgoing lf energy at the shoreline has been observed. The nonlinear energy transfer model seems to reproduce part of this behavior of energy transfer from lf components to superharmonics, at least within the surf zone. This is consistent with the works of *Thomson et al.* [2006] and *Henderson et al.* [2006]. Their finding of full reflection from the shoreline is consistent with our observations for the low group frequency (long wave groups) wave conditions. In contrast, for the high group frequency conditions, a considerably larger reduction in lf amplitude has been observed, which is not explained by nonlinear energy transfer to higher frequencies.

The analysis presented in this paper is therefore consistent with previous studies [*Van Dongeren et al.*, 2007; *de Bakker et al.*, 2015, 2016a; *Battjes et al.*, 2004] suggesting lf wave breaking as the mechanism behind the sharp reduction in ILW amplitude. In *Van Dongeren et al.* [2007] and *de Bakker et al.* [2016a,2016b], they attributed the lf wave breaking to the growth in asymmetry of the lf wave due to self-self interaction ($\{f_g, f_g\} \rightarrow 2f_g$). However, the results presented in this paper suggest that for a decreasing number n of short waves forming the group, the component $2f_g$ also becomes a subharmonic of the coupling between primary wave and the wave group components. Therefore, the growth of lf wave height and asymmetry in the nearshore areas (surf zone) is partly explained by wave group frequency self-self interaction, and partly by nonlinear coupling between primary wave components and the wave group frequency. Visually, this is explained as hf broken waves focusing (reported as bore-bore capture of short waves [*Sénéchal et al.*, 2001; *Van Dongeren et al.*, 2007] or bore merging [*Tissier et al.*, 2015]) at the crest of the lf wave motion destabilizing the lf wave and eventually breaking. The probability of this lf breaking happening, as described in this paper for the particular case $n = 3$, tends to be reduced in groups composed of an increasing number n of short waves. This behavior is consistent with the influence of β_H in the shoreline reflection coefficient R [*Battjes et al*., 2004; *Van Dongeren et al*., 2007] or ILW dissipation at the shoreline D presented here.

5. Conclusions

A detailed analysis of new experimental data for the propagation of bichromatic wave groups on a very gentle beach slope has been presented. The use of a gentle beach profile (1:100) with a high cross-shore wave gauge resolution provides a detailed analysis of nonlinear energy transfer between frequency components over a very long shoaling region. In this work, different wave conditions were generated to account for the influence of the group modulation on the hf and lf wave dynamics.

The individual wave tracking has shown a varying breakpoint location oscillating with the wave group frequency and whose amplitude affects the surf zone width. Longer wave groups (low group frequency) have shown a longer breakpoint excursion and their breaking onsets move seaward compared to the shorter wave groups. This is explained by the increasing growth of hf wave skewness during wave group shoaling, inducing an earlier hf wave breaking for low group frequency wave conditions. The different behavior of wave skewness among the studied cases is partly explained by the nonlinear energy transfers from the primary wave components to superharmonics, and partly by the transfer of energy to subharmonics, where a larger decay of the primary wave components is observed for larger group frequency wave conditions, limiting the contribution of the primary waves to the skewness.

The influence of the wave group frequency in the hf wave breaking is also observed in the hf wave height to water depth ratio γ, which is shown to increase with the group frequency. The γ coefficient computed for individual waves was shown to describe the breaking sequence remarkably well ($R^2 > 0.91$). Traditional models estimate γ using the Iribarren number ξ, which does not account for variations in the group frequency. Therefore, a modification to the Iribarren number has been proposed in this work, to account for that influence as expressed in equation (13). The proposed formulation for γ displays a good correlation with the presented data.

The growth of the ILWs in the shoaling region has confirmed previous studies in terms of amplitude and phase evolution [*Janssen et al*., 2003; *Battjes et al*., 2004; *Van Dongeren et al*., 2007]. An accurate measurement of the phase shift $\Delta\psi$, of the ILW lagging behind the hf wave structure in the nearshore areas has been achieved. The increasing phase-lag $\Delta\psi$, as the wave group frequency f_g increases, matches the ILW growth under the same conditions.

After hf wave breaking, the wave group frequency is shown to have a large impact on the lf wave dissipation. For low group frequency conditions, the hf wave modulation decay occurs over a wider surf zone, primary wave forcing still persists in the surf zone and the lf wave decay is small and caused by nonlinear energy transfer from the wave group frequency to higher frequencies. The remaining lf energy reflects at the shoreline. However, for large group frequency wave conditions, the lf wave decay is stronger and cannot be explained by energy transfer to higher frequencies. In this case, the lf wave seems to turn unstable in the inner surf zone due to the enhancement of lf components that are simultaneously superharmonics of f_g (self-self interaction) and subharmonics of triad interactions between the primary waves and the wave group frequency ($2f_g = f_2 - f_g$). In the latter case, lf wave breaking has been observed.

Acronyms

hf	high frequency
HOS	higher-order spectra
ILW	Incident Long Wave
IFLW	Incident Free Long Wave
lf	low frequency
OFLW	Outgoing Free Long Wave
ShWL	shallow water limit

Acknowledgments

The first author is supported with a PhD fellowship from the Department of Civil and Environmental Engineering, Imperial College London. Data underlying this article (IBIMS_ICL) can be accessed on zenodo at https://doi.org/10.5281/zenodo.580327, and used under the Creative Commons Attribution licence. The authors thank Marcos Rodríguez and the two reviewers for their suggestions, corrections, and useful comments.

References

Aagaard, T., and B. Greenwood (2008), Infragravity wave contribution to surf zone sediment transport—The role of advection, *Mar. Geol.*, *251*(1), 1–14, doi:10.1016/j.margeo.2008.01.017.

Alsina, J. M., and T. E. Baldock (2007), Improved representation of breaking wave energy dissipation in parametric wave transformation models, *Coastal Eng.*, *54*, 765–769, doi:10.1016/j.coastaleng.2007.05.005.

Alsina, J. M., E. M. Padilla, and I. Cáceres (2016), Sediment transport and beach profile evolution induced by bi-chromatic wave groups with different group periods, *Coastal Eng.*, *114*, 325–340, doi:10.1016/j.coastaleng.2016.04.020.

Babanin, A., D. Chalikov, I. Young, and I. Savelyev (2007), Predicting the breaking onset of surface water waves, *Geophys. Res. Lett.*, *34*, L07605, doi:10.1029/2006GL029135.

Baldock, T. E. (2012), Dissipation of incident forced long waves in the surf zone-Implications for the concept of 'bound' wave release at short wave breaking, *Coastal Eng.*, *60*, 276–285, doi:10.1016/j.coastaleng.2011.11.002.

Baldock, T. E., and D. A. Huntley (2002), Long-wave forcing by the breaking of random gravity waves on a beach, *Proc. R. Soc. London, Ser. A*, *458*(2025), 2177–2201, doi:10.1098/rspa.2002.0962.

Baldock, T. E., and D. J. Simmonds (1999), Separation of incident and reflected waves over sloping bathymetry, *Coastal Eng.*, *38*(3), 167–176, doi:10.1016/S0378-3839(99)00046-0.

Baldock, T. E., D. A. Huntley, P. A. D. Bird, T. O'Hare, and G. N. Bullock (2000), Breakpoint generated surf beat induced by bichromatic wave groups, *Coastal Eng.*, *39*, 213–242, doi:10.1016/S0378-3839(99)00061-7.

Baldock, T. E., J. A. Alsina, I. Caceres, D. Vicinanza, P. Contestabile, H. Power, and A. Sanchez-Arcilla (2011), Large-scale experiments on beach profile evolution and surf and swash zone sediment transport induced by long waves, wave groups and random waves, *Coastal Eng.*, *59*(2), 214–227, doi:10.1016/j.coastaleng.2010.10.006.

Battjes, J. A. (1974), Surf similarity, *Coastal Eng. Proc.*, *1*(14), 466–480, doi:10.1061/9780872621138.029.

Battjes, J. A., H. J. Bakkenes, T. T. Janssen, and A. R. Van Dongeren (2004), Shoaling of subharmonic gravity waves, *J. Geophys. Res.*, *109*, C02009, doi:10.1029/2003JC001863.

Biésel, F. (1952), Équations générales au second ordre de la houle irrégulière, *La Houille Blanche*, *3*, 372–376, doi:10.1051/lhb/1952033.

Bowen, A. J., D. L. Inman, and V. P. Simmons (1968), Wave 'set-down' and set-up, *J. Geophys. Res.*, *73*, 2569–2577, doi:10.1029/JB073i008p02569.

Bowers, E. C. (1977), Harbour resonance due to set-down beneath wave groups, *J. Fluid Mech.*, *79*, 71–92, doi:10.1017/S0022112077000044.

Contardo, S., and G. Symonds (2013), Infragravity response to variable wave forcing in the nearshore, *J. Geophys. Res. Oceans*, *118*, 7095–7106, doi:10.1002/2013JC009430.

de Bakker, A. T. M., M. F. S. Tissier, and B. G. Ruessink (2014), Shoreline dissipation of infragravity waves, *Cont. Shelf Res.*, *72*, 73–82, doi:10.1016/j.csr.2013.11.013.

de Bakker, A. T. M., T. H. C. Herbers, P. B. Smit, M. F. S. Tissier, and B. G. Ruessink (2015), Nonlinear infragravity-wave interactions on a gently sloping laboratory beach, *J. Phys. Oceanogr.*, *45*(2), 589–605, doi:10.1175/JPO-D-14-0186.1.

de Bakker, A. T. M., M. F. S. Tissier, and B. G. Ruessink (2016a), Beach steepness effects on nonlinear infragravity-wave interactions: A numerical study, *J. Phys. Oceanogr.*, *121*(1), 554–570, doi:10.1002/2015JC011268.

de Bakker, A. T. M., J. A. Brinkkemper, F. van der Steen, M. F. S. Tissier, and B. G. Ruessink (2016b), Cross-shore sand transport by infragravity waves as a function of beach steepness, *J. Geophys. Res. Earth Surf.*, *121*, 1786–1799, doi:10.1002/2016JF003878.

Doering, J. C., and A. J. Bowen (1986), Shoaling surface gravity waves: A bispectral analysis, in *Proceedings of the 20th International Conference Coastal Engineering*, pp. 150–162, ASCE, Taipei, Taiwan, doi:10.1061/9780872626003.012.

Doering, J. C., and A. J. Bowen (1995), Parameterization of orbital velocity asymmetries of shoaling and breaking waves using bispectral analysis, *Coastal Eng.*, *26*(1), 15–33, doi:10.1016/0378-3839(95)00007-X.

Dong, G. H., X. Z. Ma, J. W. Xu, Y. X. Ma, and G. Wang (2009), Experimental study of the transformation of bound long waves over a mild slope with ambient currents, *Coastal Eng.*, *56*(10), 1035–1042, doi:10.1016/j.coastaleng.2009.06.010.

Elgar, S., and R. T. Guza (1985), Observations of bispectra of shoaling surface gravity waves, *J. Fluid Mech.*, *161*, 425–448, doi:10.1017/S0022112085003007.

Elgar, S., and R. T. Guza (1986), Nonlinear model predictions of bispectra of shoaling surface gravity waves, *J. Fluid Mech.*, *167*, 1–18, doi:10.1017/S0022112086002690.

Elgar, S., T. H. C. Herbers, M. Okihiro, J. Oltman-Shay, and R. T. Guza (1992), Observations of infragravity waves, *J. Geophys. Res.*, *97*, 15,537–15,577, doi:10.1029/92JC01316.

Guedes, R., K. R. Bryan, and G. Coco (2013), Observations of wave energy fluxes and swash motions on a low-sloping, dissipative beach, *J. Geophys. Res. Oceans*, *118*, 3651–3669, doi:10.1002/jgrc.20267.

Guza, R. T., and E. B. Thornton (1982), Swash oscillations on a natural beach, *J. Geophys. Res.*, *87*, 483–491, doi:10.1029/JC087iC01p00483.

Hasselmann, K., W. Munk, and G. MacDonald (1963), Bispectra of ocean waves, in *Time Series Analysis*, Chapter 8, pp. 125–139, Wiley, New York.

Henderson, S. M., R. T. Guza, S. Elgar, T. H. C. Herbers, and A. J. Bowen (2006), Nonlinear generation and loss of infragravity wave energy, *J. Geophys. Res.*, *111*, C12007, doi:10.1029/2006JC003539.

Herbers, T. H. C., S. Elgar, and R. T. Guza (1995), Generation and propagation of infragravity waves, *J. Geophys. Res.*, *100*, 24,863–24,872, doi:10.1029/95JC02680.

Herbers, T. H. C., N. R. Russnogle, and S. Elgar (2000), Spectral energy balance of breaking waves within the surf zone, *J. Phys. Oceanogr.*, *30*(11), 2723–2737, doi:10.1175/1520-0485(2000)030<2723:SEBOBW>2.0.CO;2.

Janssen, T. T., J. A. Battjes, and A. R. Van Dongeren (2003), Long waves induced by short-wave groups over a sloping bottom, *J. Geophys. Res.*, *108*(C8), 3252, doi:10.1029/2002JC001515.

Johannessen, T. B., and C. Swan (2003), On the nonlinear dynamics of wave groups produced by the focusing of surface-water waves, *Proc. R. Soc., London, Ser. A*, *459*(2032), 1021–1052, doi:10.1098/rspa.2002.1028.

Jonsson, I. G. (1966), Wave boundary layers and friction factors, *Coastal Eng. Proc.*, *1*(10), 127–148, doi:10.1061/9780872620087.010.

Kostense, J. K. (1984), Measurements of surf beat and set-down beneath wave groups, *Coastal Eng. Proc.*, *1*(19), 724–740, doi:10.1061/9780872624382.050.

Lara, J. L., A. Ruju, and I. J. Losada (2011), Reynolds averaged Navier-stokes modelling of long waves induced by a transient wave group on a beach, *Proc. R. Soc. A*, *467*, 1215–1242, doi:10.1098/rspa.2010.0331.

List, J. H. (1991), Wave groupiness variations in the nearshore, *Coastal Eng.*, *15*(5–6), 475–496, doi:10.1016/0378-3839(91)90024-B.

List, J. H. (1992), A model for the generation of two-dimensional surf beat, *J. Geophys. Res.*, *97*, 5623–5635, doi:10.1029/91JC03147.

Longuet-Higgins, M. S., and R. W. Stewart (1962), Radiation stress and mass transport in gravity waves, with application to 'surf beats', *J. Fluid Mech.*, *13*, 481–504, doi:10.1017/S0022112062000877.

Longuet-Higgins, M. S., and R. W. Stewart (1964), Radiation stresses in water waves: A physical discussion, with applications, *Deep Sea Res. Oceanogr. Abstr.*, *11*(4), 529–562, doi:10.1016/0011-7471(64)90001-4.

Moura, T., and T. E. Baldock (2017), Remote sensing of the correlation between breakpoint oscillations and infragravity waves in the surf and swash zone, *J. Geophys. Res. Oceans*, *122*, 3106–3122, doi:10.1002/2016JC012233.

Norheim, C. A., T. H. C. Herbers, and S. Elgar (1998), Nonlinear evolution of surface wave spectra on a beach, *J. Phys. Oceanogr.*, *28*, 1534–1551, doi:10.1175/1520-0485(1998)028<1534:NEOSWS>2.0.CO;2.

Padilla, E. M., and J. M. Alsina (2016), Laboratory experiments of bichromatic wave groups propagation on a gentle beach profile and energy transfer to low and high frequency components, in Proceedings of the 35th International Conference on Coastal Engineering, (Istanbul, Turkey), ASCE, 1(35), 6, doi:10.9753/icce.v35.currents.6.

Phillips, O. M. (1960), On the dynamics of unsteady gravity waves of finite amplitude: Part 1. The elementary interactions, *J. Fluid Mech.*, *9*, 193–217, doi:10.1017/S0022112060001043.

Rocha, M. V. L., H. Michallet, and P. A. Silva (2017), Improving the parameterization of wave nonlinearities—The importance of wave steepness, spectral bandwidth and beach slope, *Coastal Eng.*, *121*, 77–89, doi:10.1016/j.coastaleng.2016.11.012.

Ruessink, B. G., M. G. Kleinhans, and P. G. L. den Beukel (1998), Observations of swash under highly dissipative conditions, *J. Geophys. Res.*, *103*, 3111–3118, doi:10.1029/97JC02791.

Schäffer, H. A. (1993), Infragravity waves induced by short-wave groups, *J. Fluid Mech.*, *247*, 551–588, doi:10.1017/S0022112093000564.

Schäffer, H. A., and I. G. Jonsson (1990), Theory versus experiments in two-dimensional surf beat, *Coastal Eng. Proc.*, *1*(22), 1131–1143, doi:10.9753/icce.v22.%25p.

Sénéchal, N., P. Bonneton, and H. Dupuis (2001), Field observations of irregular wave transformation in the surf zone, *Coastal Dyn.*, *1*, 62–71, doi:10.1061/40566(260)7.

Sénéchal, N., G. Coco, K. R. Bryan, and R. A. Holman (2011), Wave runup during extreme storm conditions, *J. Geophys. Res.*, *116*, C07032, doi:10.1029/2010JC006819.

Spinneken, J., and C. Swan (2011), Theoretical transfer function for force-controlled wave machines, *Int. J. Offshore Polar Eng.*, *21*(3), 169–177.

Stokes, G. G. (1847), On the theory of oscillatory waves, *Trans. Cambridge Philos. Soc.*, *8*, 441–455.

Symonds, G., and A. J. Bowen (1984), Interactions of nearshore bars with incoming wave groups, *J. Geophys. Res.*, *89*, 1953–1959, doi:10.1029/JC089iC02p01953.

Symonds, G., D. A. Huntley, and A. J. Bowen (1982), Two-dimensional surf beat: Long wave generation by a time-varying breakpoint, *J. Geophys. Res.*, *87*, 492–498, doi:10.1029/JC087iC01p00492.

Thomson, J., S. Elgar, B. Raubenheimer, T. H. C. Herbers, and R. T. Guza (2006), Tidal modulation of infragravity waves via nonlinear energy losses in the surfzone, *Geophys. Res. Lett.*, *33*, L05601, doi:10.1029/2005GL025514.

Thornton, E. B., and R. T. Guza (1982), Energy saturation and phase speeds measured on a natural beach, *J. Geophys. Res.*, *87*, 9499–9508, doi:10.1029/JC087iC12p09499.

Tissier, M., P. Bonneton, H. Michallet, and B. G. Ruessink (2015), Infragravity-wave modulation of short-wave celerity in the surf zone, *J. Geophys. Res. Oceans*, *120*, 6799–6814, doi:10.1002/2015JC010708.

Van Dongeren, A. R., and I. A. Svendsen (1997), *Quasi 3-D Modeling of Nearshore Hydrodynamics (*No. *CACR-97–04)*, Cent. for Appl. Coastal Res., Univ of Delaware, Nemark.

Van Dongeren, A. R., H. J. Bakkenes, and T. Janssen (2002), Generation of long waves by short wave groups, in *Proceedings of the 28th International Conference on Coastal Engineering*, pp. 1093–1105, ASCE, Wales, U. K.

Van Dongeren, A. R., J. Battjes, T. T. Janssen, J. Van Noorloos, K. Steenhauer, G. Steenhauer, and A. J. H. M. Reniers (2007), Shoaling and shoreline dissipation of low-frequency waves, *J. Geophys. Res.*, *112*, C02011, doi:10.1029/2006JC003701.

Veeramony, J., and I. A. Svendsen (1996), Wave groups in the surf-zone: Model and experiments, *Coastal Eng. Conf.*, *1*, 151–164, doi:10.1061/9780784402429.012.